

ASSESSING PALAEOLOSOL MATURITY IN FLUVIAL SETTINGS: THE PENNSYLVANIAN MUDSTONE SERIES, POLISH PART OF THE UPPER SILESIAN BASIN

Patrycja TOMALA¹, Artur KULIGIEWICZ^{1*}, Richard LOJKA²,
Weronika NADŁONEK³, Beata NAGLIK³ & Artur KĘDZIOR¹

¹ Institute of Geological Sciences, Polish Academy of Sciences, Senacka 1, 31-002 Kraków, Poland,
e-mails: ppatrycja201@gmail.com, ndkuligi@cyf-kr.edu.pl, ndkedzio@cyf-kr.edu.pl

² Czech Geological Survey, Klárov 3/131, 118 21 Praha 1, Czech Republic,
e-mail: richard.lojka@geology.cz

³ Polish Geological Institute-National Research Institute, Upper Silesian Branch,
Królowej Jadwigi 1, 41-200 Sosnowiec, Poland,
e-mails: wnad@pgi.gov.pl, bnag@pgi.gov.pl

* Corresponding author

Tomala, P., Kuligiewicz, A., Lojka, R., Nadłonek, W., Naglik, B. & Kędzior, A., 2026. Assessing palaeosol maturity in fluvial settings: the Pennsylvanian Mudstone Series, Polish part of the Upper Silesian Basin. *Annales Societatis Geologorum Poloniae*, 96: 67–90.

Abstract: Palaeosols preserved within the Mudstone Series of the Upper Silesian Basin offer a potential archive of Pennsylvanian environmental conditions, yet they remain largely uncharacterized. The aim of this study was to evaluate whether these mineral palaeosol horizons can reliably record palaeoenvironmental and palaeoclimatic signals, despite their fluvial depositional setting and subsequent diagenetic overprint. Palaeosols from selected intervals of six cores were described macroscopically and investigated, using micromorphological analysis, X-ray diffraction, scanning electron microscopy (SEM), and bulk-rock geochemistry. The palaeosol profiles are thin and weakly developed. Most consist of a massive or weakly structured C horizon and a single mineral B horizon, overlain by a coal seam (H horizon). They were classified as gleyed Protosols. Micromorphology revealed frequent preservation of primary lamination, limited pedogenic aggregation, and rare other pedogenic features, such as slickensides and clay skins. SEM analyses documented *in situ* pedogenic and early diagenetic siderite, as well as accessory minerals (galena, pyrite, sphalerite, barite), commonly associated with organic matter. Mineralogically, the palaeosols are dominated by phyllosilicates (kaolinite, illite-smectite, and muscovite) and quartz, with a smaller content of feldspars, chlorite, and carbonates. The mineralogical variability between boreholes was low. Geochemical proxies (CIW > 90, high CALMAG, elevated Rb/Sr and low Sr/Cu ratios; ω - ψ and RW indices) consistently indicate strong weathering and a predominantly felsic provenance, with most samples plotting as highly weathered, relative to reference profiles. However, these indices contradict the weak pedogenic development observed microscopically, implying that the chemical signatures predominantly reflect pre-depositional weathering in the broader catchment, rather than *in situ* soil-forming processes. Frequent flooding strongly prohibited the development of highly mature and differentiated soil profiles, which effectively limits the utility of the material investigated as a direct palaeoclimate archive.

Key words: Palaeosols, Upper Silesian Basin, chemical weathering, maturity, Pennsylvanian.

Manuscript received 30 November 2025, accepted 12 June 2026

INTRODUCTION

The characterization of fossilized soils, or palaeosols, can provide important information about the palaeoenvironmental conditions that influenced soil formation in the geologic past (Singer, 1980; Sheldon and Tabor, 2009; Tabor and Myers, 2015). The rate of the pedogenic process can vary over a wide range, as it is a function of many variables, including substrate type, climate, biological activity, drainage

conditions, and topography (Weil and Brady, 2017). The more mature palaeosols are, the more information on their formation environment might be obtained (Tabor *et al.*, 2017). The term “mature palaeosol” is, however, somewhat arbitrary and lacks a strict formal definition, which is understandable, given the great variability of palaeosols. In the classification of Mack *et al.* (1993), designed for

pre-Quaternary palaeosols, a palaeosol is classified as Protosol (i.e., an immature soil, corresponding to Inceptisol or Entisol in the USDA Soil Taxonomy), when pedogenic features, such as horizonation, ped structure, argillans or pedogenic carbonate concretions are insufficiently developed for any of them to be the dominant feature of the profile. There is a general consensus that a palaeosol is immature, if the pedogenic features are weakly developed. However, there is no universal definition of “weak development”, as palaeosol features are descriptive and, therefore, subjective (Sheldon and Tabor, 2009; Tabor and Myers, 2015). This implies that the “maturity” vs. “immaturity” of palaeosol horizons has to be assessed on a case-by-case basis, taking into account the particular palaeosol type and geologic context. However, in some cases, even apparently “mature” palaeosols may not provide useful data on palaeoclimate, e.g., because of climatic signal shredding, due to erosion or reworking (e.g., Jewuła *et al.*, 2026) or diagenesis (e.g., Kuligiewicz *et al.*, 2021; McIntosh *et al.*, 2023). The former is particularly likely to occur in fluvial environments, where floodplain soils, developing on fine-grained (i.e., “pre-weathered”) material, are prone to frequent rejuvenation by flooding (Singer, 1980). Soils developed under a moisture deficit, such as Gelisols (where moisture occurs only during the thawing season) or Aridisols (soils developed in desert settings) also usually imprint biased information on the climatic conditions, because weathering occurs only during the warm season (Gelisols) or when moisture is available (Aridisols).

The Late Mississippian and Pennsylvanian were periods, during which large coal deposits accumulated in equatorial sedimentary basins, including the foreland of the Variscan orogen (Opluštil and Cleal, 2007; DiMichele *et al.*, 2010). The Upper Silesian Basin (USB), located on the border of Czechia and Poland, contains up to 8,500 m of coal-bearing strata, accumulated between the Namurian A and Westphalian D stages (Kędzior *et al.*, 2007). The Mudstone Series (MS) comprises up to 2,000 m of mudstone-dominated strata, deposited by meandering river systems (Doktor and Gradziński, 1985; Kędzior *et al.*, 2025). Besides coal seams, a large number of mineral palaeosol horizons were formed on the alluvial plains of these river systems. However, to date, little attention has been paid to these palaeosol horizons, which remain generally poorly characterized. Filling this research gap will allow a better understanding of the environmental conditions, prevailing during the deposition of the MS.

The parent material of palaeosols in the MS was alluvia, accumulated on the floodplains. This predominantly fine-grained material underwent further *in situ* weathering during late Carboniferous pedogenesis. During pedogenesis in such environments, feldspar, micas, and chlorite are transformed into kaolinite and expandable clay minerals (Churchman and Lowe, 2012). Simultaneously, iron (hydr) oxides are likely to precipitate, along with siderite and/or sulphates, depending on the redox state of the deeper parts of the soil column. Mineralogical changes are reflected in the changes in the chemical composition of the material, which is progressively depleted in mobile base elements, such as Mg, Ca, K, and Na (Tabor and Myers, 2015). The intensity of such mineralogical and chemical transformation

depends on the climatic conditions and the duration of surface exposure. Estimating the chemical weathering indices and element ratios, based on palaeosols from terrestrial environments, therefore, contributes to the reconstruction of the palaeoenvironmental conditions and reflects climate changes in the past (Sheldon and Tabor, 2009; Huang *et al.*, 2010; Zhang *et al.*, 2021). Palaeoclimatic information can also be extracted from the ratios of minor and trace elements. The values of the Sr/Cu, Rb/Sr, and Sr/Ba ratios in sedimentary rocks should allow the determination of climatic conditions, because Sr is more soluble and more easily leached in palaeosols than Cu, Rb, and Ba (Nesbitt and Young, 1982; Retallack, 2008; Kahmann-Robinson *et al.*, 2008; Zhang *et al.*, 2018). Rubidium occurs mainly in K-feldspars, micas, and clay minerals, while strontium occurs in plagioclases, amphiboles, pyroxenes, and carbonate minerals (Ouyang *et al.*, 2019).

The aim of the present work was to determine if palaeosol horizons in the MS of the USB are capable of providing information on the climatic conditions, prevailing during the accumulation of the sediments of this stratigraphic unit, given their geological setting. In order to achieve this, thirty-five palaeosol horizons were identified in available cores. The palaeosols underwent detailed examination, including geochemical, mineralogical, and micromorphological analyses. An attempt was made to evaluate which of these methods provides the most reliable information for assessing palaeosol maturity in this particular time slice in the USB, considering its depositional and diagenetic history.

GEOLOGICAL SETTING

The Upper Silesian Basin is one of the largest coal-bearing basins in Europe. It is located in the foreland position of the advancing Variscan orogen from the west. The total area of the basin is approximately 7,400 km², including approximately 5,600 km² in Poland (Fig. 1). The current shape of the basin is a result of the Variscan tectonics, modified later by Alpine orogeny as well as post-Carboniferous erosion. The present-day basin is bounded in the west by the Variscan Devonian to Mississippian nappe complex, on the NE side by the Kraków-Lubliniec strike-slip fault zone. The southern extent of the basin is known only from scarce boreholes that penetrated the coal-bearing succession through the overlying Carpathian nappes and their Miocene foredeep deposits. The Upper Mississippian-Pennsylvanian foredeep infill of the USB consists of pre-coal-bearing Mississippian flysch-type deposits that transition through the Upper Mississippian to the molasse-type coal-bearing succession. The bipartite coal-bearing succession exhibits differences with regard to the occurrence of a marine fauna. The Upper Mississippian deposits of the Paralic Series were accumulated in fluvial and complex coastal systems with numerous marine, brackish, and freshwater fauna horizons (Gradziński *et al.*, 2005; Opluštil *et al.*, 2024). This series is characterized by the cyclic alternation of marine and continental siliciclastics and contains tuffite horizons (Jirásek *et al.*, 2013) and is separated from the overlying Pennsylvanian succession by a stratigraphic gap (Kotas,



Fig. 1. A simplified geological map of the Upper Silesian Basin (USB) after Jureczka *et al.* (1995), with the locations of the investigated boreholes.

1995). The Pennsylvanian succession is characterized by the absence of marine horizons and is considered to be entirely continental. This part is further subdivided into the Upper Silesian Sandstone, Mudstone, and Cracow Sandstone series. The Upper Silesian Sandstone Series, regarded as deposited within braided to meandering fluvial systems, is separated from underlying Mississippian deposits by a stratigraphic gap (Jureczka and Kotas, 1995; Kędzior *et al.*, 2007; Kędzior, 2016) and is overlain by the Mudstone Series sediments. The lower boundary of this unit is placed at the top of the freshwater fauna horizon. The Mudstone Series is dominated by fine-grained deposits, accumulated on the vast alluvial plain, constructed by meandering and possibly anastomosing fluvial systems (Doktor and Gradziński, 1985). The transition to the overlying Cracow Sandstone Series is usually sharp and marked by the occurrence of thick

sandstone bodies that alternate periodically with basin-wide mudstone deposits (Kotas, 1995; Laurin *et al.*, 2024). The Cracow Sandstone series, which is the last coal-bearing series of the USB, was deposited by braided river systems (Doktor, 2007). The Cracow Sandstone Series is overlain by the coal-barren Kwaczała Arkose, which occurs only in the eastern part of the USB. The Kwaczała Arkose consists of coarse-grained, poorly lithified, arkosic sandstones and conglomerates with red and variegated shale interbeds. The maximum thickness of the coal-bearing succession is noted in the western part of the basin, with a distinct, gradual decrease of thickness towards the east. The combined thickness of coal-bearing formations is 8,500 m.

The Mudstone Series (Westphalian A and B) is divided into two units: the older Załęże Beds and the younger Orzesze Beds (Kotas, 1995), with the boundary at a pyroclastic

horizon, or at the top of the 328 coal seam. The Mudstone Series occupies the largest area among the continental sediments of the coal-bearing Carboniferous in the USB (Fig. 1). Sediments of the Mudstone Series occur in the central and eastern parts of the basin, spanning an area that is 80 km in length and 50 km in width. The maximum recorded thickness is up to 2,000 m in the western parts, and it gradually thins eastward to 150 m. It predominantly consists of fine-grained clastic sediments, including mudstones, sandy mudstones, and subordinate claystones, with incorporated, fine- to medium-grained, ribbon-like sandstone bodies, deposited on the alluvial plain of the meandering and anastomosing river systems (Doktor and Gradziński, 1985; Kędzior *et al.*, 2025). There are almost 160 coal seams, 70 of which are of economic importance (Kotas, 1995). The seams are relatively thin (rarely exceeding 1.5 m) and often contain clastic layers. The maximum thickness of coal seams occurs at the bottom of the series (seam 405).

Palaeosols in the USB have been studied mostly from a sedimentological perspective (e.g., Doktor and Gradziński, 1985; Gradziński *et al.*, 2005). Only relatively recently, Opluštil *et al.* (2019) provided a more detailed description of the palaeosols of the Cracow Sandstone Series. It was demonstrated that the palaeosols in that series record the allogenic cyclicity, caused by the changes from a seasonal climate, represented by Vertisols, to a humid climate, under which Histosols (represented by coal seams) were formed. Superposed on that cyclicity was the long-term climate evolution towards a more cyclic and drier climate, as evidenced by the cessation of peat formation at the Middle-Late Pennsylvanian boundary.

MATERIALS AND METHODS

Materials

Cores from five boreholes, Jaworzno G-5109 (JAW5109), Warszawice-Pawłowice Texaco A (WP TXA), Amoco-Miedzna 1 (AMIE), Amoco-Poręba 1 (APOR), Żory 1M (ZORIM), and Dąb-Zachód G-15 (G15), located in the southwest and northeast of the Polish part of the USB, were studied (Figs 1 and 2). Palaeosols in the cores were identified and described in detail, following the criteria established by Retallack (2008) and Kraus (1999). Briefly, palaeosol horizons were defined on the basis of changes in pedogenic or sedimentary structure, colour, pedogenic mineral accumulations, and grain size. The designation of master horizons (e.g., H, B, C) and subordinate descriptors (e.g., ss, k, g) follows the definitions in the USDA Soil Taxonomy system (Soil Survey Staff, 2022). The descriptive terms and classification scheme utilized herein follow the palaeosol-specific system of Mack *et al.* (1993). Representative palaeosol matrix samples from each horizon were collected for further mineralogical, petrological, and geochemical analysis. In total, 38 samples were collected. Thirty-three of them come from the MS, with the remaining 5 collected from the Cracow Sandstone Series (CSS; Dąb-Zachód G-15 borehole). Samples from the CSS represent the Libiąż Beds. The MS samples have been collected mainly from Załęże Beds, with the exception of samples from the AMIE

borehole, which belonged to Orzesze Beds. The studied intervals are listed in Table 1.

Analytical Methods

Optical Microscope

Petrographic thin sections were prepared in the IGS PAS and PGI-NRI laboratories from selected samples. Thin sections were prepared perpendicular to the bedding. The thin sections were analyzed using a Nikon Eclipse E600 POL microscope under plane and cross-polarized light. The thin sections were described following the terminology of Stoops *et al.* (2010).

Scanning Electron Microscope

Selected thin sections were also carbon-coated and analyzed, using scanning electron microscopy (SEM). The backscattered electron (BSE) observations were performed on polished samples, using a Hitachi SU3500 scanning electron microscope in the variable-pressure mode. The accelerating voltage was set to 15 kV, the working distance to 10 mm, and the spot size (probe current) to 70 (dimensionless unit provided by the SEM software). The chemical composition of minerals was obtained by semi-quantitative analysis with the Thermo Scientific UltraDry compact EDS detector at the Polish Geological Institute-National Research Institute or using the field emission scanning electron microscope Hitachi S-4700, equipped with the energy-dispersive X-ray (EDS) Noran Vantage system, operating with an accelerating voltage of 20 kV, at the Institute of Geological Sciences, Jagiellonian University.

X-Ray Diffraction (XRD)

For mineralogical analyses, samples were crushed in a ceramic mortar with a pestle to pass through a 0.45 mm sieve. Portions of selected samples were subjected to a series of chemical treatments, following the procedure of Jackson (1969), which included reactions with a sodium acetate-acetic acid buffer (pH = 5.5), sodium hypochlorite, and sodium dithionite-citrate-bicarbonate (DCB) solution (Mehra and Jackson, 1960), which removed carbonates, organic matter, and poorly crystalline iron (hydr)oxides, respectively. Subsequently, the <2 µm size fraction was separated by centrifugation. Aliquots of <2 µm size fractions were saturated with Ca²⁺ or K⁺ by three washings with a 1 M solution of the appropriate chloride, followed by dialysis and oven-drying at 60°C.

X-ray diffraction (XRD) patterns of random powder mounts were obtained with a Rigaku SmartLab SE diffractometer, equipped with a Cu lamp, a CBO- α accessory, and an Ni filter in the 2-65°2 θ range, with a 0.02° step and a 1 s counting time. Random powder mounts were prepared from raw samples that passed through a 0.45 mm sieve and were milled in methanol in a McCrone micronizing mill. XRD patterns of oriented Ca²⁺ and K⁺ exchanged <2 µm size fractions were registered, using the same experimental settings. Ca-exchanged specimens were analyzed in air-dried (AD) and ethylene glycol-solvated (EG) states, while K-exchanged samples were registered in the AD state and after heating for 1 h at 330°C and 550°C. Quantitative analysis of

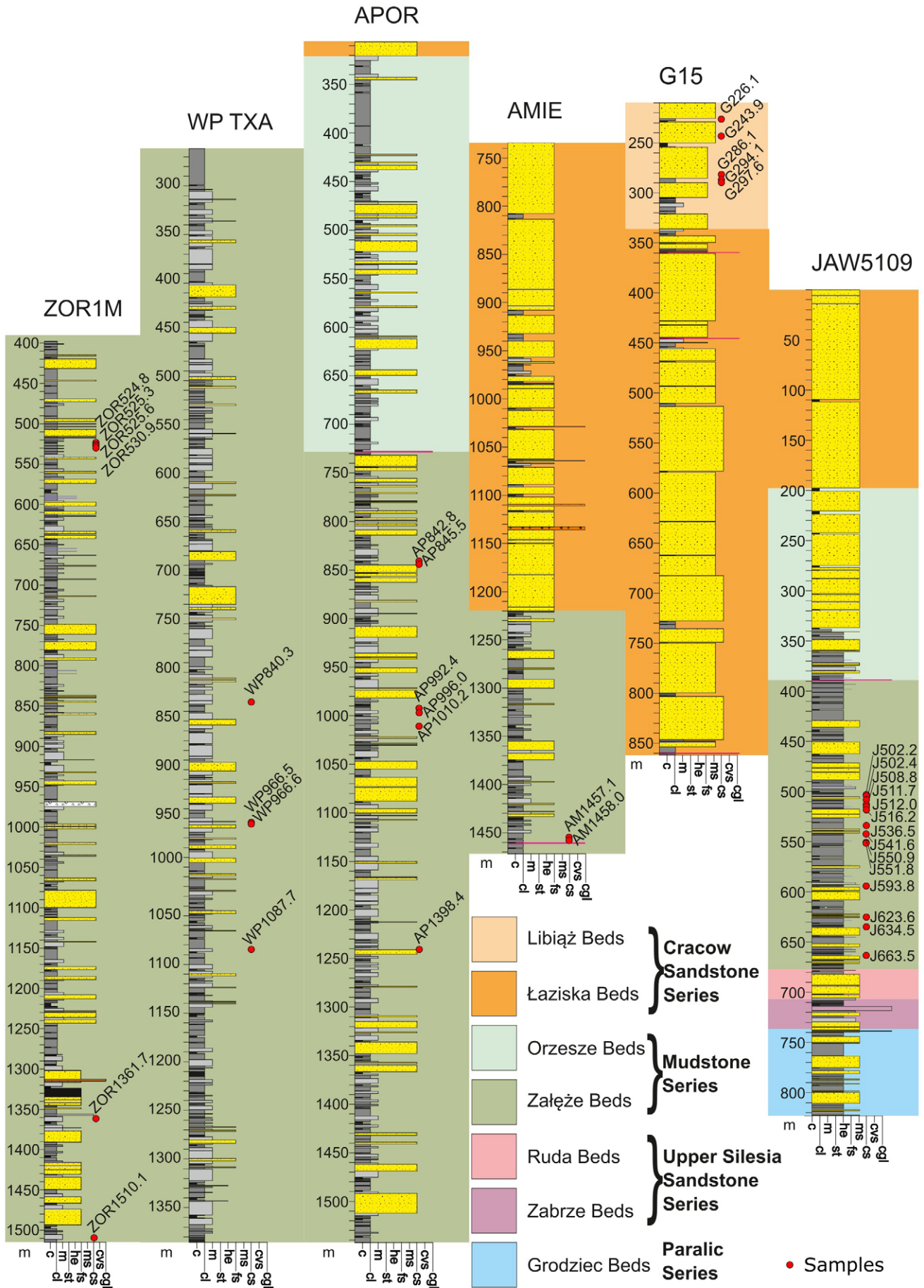


Fig. 2. Lithostratigraphic sections of the boreholes investigated, with the locations of the studied palaeosol horizons.

Table 1

Sample list with depths.

Borehole	Stratigraphy	Sample name	Depth in core (m)	Depth in palaeosol (cm)	Palaeosol horizon	Palaeosol type
Dąb-Zachód G-15 (G15)	Cracow Sandstone Series (Libiąż Beds) Mudstone Series (Załęże Beds)	G226.1	226.0–226.1	15	Bg	gleyed Protosol
		G243.9	243.8–243.9	10	Bw	
		G286.1	286.0–286.1	80	Bssg	
		G294.1	294.0–294.1	25	Bw	
		G297.6	297.5–297.6	100	Bw	
Jaworzno G-5109 (JAW5109)		J498.3	498.30–498.35	n.a.*	Bw	
		J502.2	502.2		Bw	
		J502.4	502.4		Bw	
		J508.8	508.8		Bw	
		J511.7	511.75		Bw	
		J512.0	512.0–511.9		Bw	
		J516.2	516.20–516.25		Bw	
		J536.5	536.40–536.50		Bw	
		J541.6	541.65		Bw	
		J550.9	550.90–550.80		Bw	
J551.8	551.7–551.8	Bw				
J593.8	593.8	Bw				
J623.6	623.6	Bw				
J634.5	634.5	Bw				
J663.5	663.5	Bw				
Warszowice-Pawłowice Texaco A (WP TXA)	W840.3	840.2–840.3	10	Bw		
	W966.5	966.4–966.5	20	Bw		
	W966.6	966.5–966.6	30	Bssg		
	W1087.7	1087.6–1087.7	10	Bg		
Amoco-Miedźna 1 (AMIE)	Mudstone Series (Orzesze Beds)	AM1457.1	1457.0–1457.1	10	Bw	
		AM1458.0	1457.9–1458	10	Bw	
Amoco-Poręba 1 (APOR)	Mudstone Series (Załęże Beds)	AP842.8	842.7–842.8	10	Bw	
		AP845.5	845.5–845.4	180	Bw	
		AP992.4	992.3–992.4	20	Bw	
		AP996.0	995.9–996.0	90	Cg	
		AP1010.2	1010.1–1010.2	25	Bw	
		AP1398.4	1398.3–1398.4	50	Bw	
Żory 1-M (ZOR1M)	Mudstone Series (Załęże Beds)	ZOR524.8	524.7–524.8	100	Bg	
		ZOR525.3	525.2–525.3	120	Bssg	
		ZOR525.6	525.5–525.6	140	BCg	
		ZOR530.9	530.8–530.9	30	Bssg	
		ZOR1361.7	1361.6–1361.7	20	Bw	
ZOR1510.1	1510.0–1510.1	70	Bssg			

the bulk palaeosol samples was performed, using the Rietveld refinement method with Profex-BGMN software (Doebelin and Kleeberg, 2015).

Geochemical analyses

Geochemical analyses of the major elements, as well as Mn, Cr, Ti, and Zn, were performed, using Inductively Coupled Plasma Optical Emission Spectroscopy (ICP-OES) or, for selected samples and elements, by Wavelength Dispersive X-Ray Fluorescence (WD-XRF). Minor and trace elements (except for Nb and Zr) were determined with inductively coupled plasma mass spectrometry (ICP-MS).

Samples for ICP-OES and ICP-MS measurements were air-dried and ground to a grain size <0.063 mm. Subsequently, they were dissolved in reactions with hot concentrated HF, HNO₃, HClO₄, and aqua regia. The ICP-OES measurements were done, using a Thermo Scientific iCAP 6500 DUO ICP-OES spectrometer. The expanded uncertainty of the results was 30%, with an assumed 95% confidence level and expansion factor of $k = 2$. The detection limits were 0.003% (Na), 0.002% (P), 0.01% (Al, Ca, Fe, K, Mg), 1 ppm (Cr, Zn), 2 ppm (Mn) and 5 ppm (Ti). ICP-MS was done, using a Perkin Elmer Elan DRC II spectrometer. The expanded uncertainty of the results was 25%, with an assumed 95% confidence level and expansion factor $k = 2$. The detection limits were: 0.05 ppm (Ba, Cu, Mo, Rb, U, Th), 0.50 ppm (Ni, La, Y), 0.10 ppm (Sr) and 1 ppm (V).

For WD-XRF, samples were fused with lithium metaborate or a mixture of lithium tetraborate and lithium metaborate, depending on a prior-determined loss on ignition (LOI). The measurements were done, using a Philips WD-XRF PW 2400 spectrometer. The expanded uncertainty of the results was 50%, with an assumed 95% probability level and an expansion factor of $k = 2$. The detection limit was 0.10%. Trace element analyses (Nb, Zr) were also done, using the WD-XRD technique with the same apparatus on pressed pellets, prepared by mixing crushed samples with Merck Hoechst C wax. The expanded uncertainty of the results was 60% and 50%, respectively, with an assumed 95% confidence level and an expansion factor of $k = 2$. The detection limit was 2 ppm. All chemical analyses were carried out in the PGI-NRI Chemical Laboratory, in Warsaw.

The resulting amounts of oxides (molecular proportions of oxides) were used to calculate the Chemical Index of Weathering (CIW), Calcium-Magnesium Weathering Index (CALMAG), Base loss, and Ruxton Ratio, according to the following formulae:

$$CIW = \frac{Al_2O_3}{Al_2O_3 + CaO + Na_2O} \times 100$$

(Harnois, 1988)

$$CALMAG = \frac{Al_2O_3}{Al_2O_3 + CaO + MgO} \times 100$$

(Nordt and Driese, 2010)

$$Base\ Loss = \frac{CaO + MgO + Na_2O + K_2O}{TiO_2}$$

(Sheldon and Tabor, 2009)

$$R = \frac{TiO_2}{Al_2O_3}$$

(Ruxton, 1968)

The CALMAG index was originally proposed specifically for Vertisols. However, it has since been used for other types of palaeosol (Andrews *et al.*, 2017). The chemical composition of samples was also evaluated in the ω - ψ space of Lipp *et al.* (2020) and the robust weathering index (RW index) of Cho and Ohta (2022). Both of these approaches use multiple major elements to extract information about the degree of weathering and the source composition of a sample set. Furthermore, in both approaches, major element concentrations first undergo a log-ratio transformation (Aitchinson, 1982) to remove the closure effects and thus allow compositional variation to be treated statistically. Lipp *et al.* (2020), using principal component analysis (PCA), demonstrated that 80% of the variation in their reference geochemical sample set could be explained by two principal components: one corresponding to magmatic differentiation, and the second to the degree of weathering. In the ω - ψ approach, the geochemical composition of a sediment sample is expressed in ω - ψ coordinates, with ψ representing the position along a mafic-felsic spectrum and ω quantifying the degree of depletion in mobile elements and thus the extent of weathering. The RW index of Cho and Ohta (2022) operates using a similar principle, but differs in the set of elements used (Ti, Al, Fe, Mg, Na, and K, instead of Si, Ti, Al, Fe, Mg, Ca, Na, and K, used in the ω - ψ approach), the type of the log-ratio transformation (isometric log-ratio instead of centered log-ratio) and the statistical treatment of data, used for the development of the index (independent component analysis, instead of PCA). In the approach proposed by Cho and Ohta (2022), two signals (parent and weathering) are also separated. However, the results are presented on a ternary diagram with apices, corresponding to the mafic, felsic, and weathering components. In addition, Rb/Sr, Sr/Cu, Sr/Ba, La/Th, TiO₂/Al₂O₃, Th/U and V/Cr ratios were calculated. Statistical calculations were performed in the R Language and Environment for Statistical Computing (R Core Team, 2024), using RStudio software.

RESULTS

Lithology

Palaeosols of the MS and the lower part of the CSS were developed on fine-grained floodplain deposits, composed of the organic-rich clastics of crevasse splays and subordnately oxbows, interlayered with the organic matter accumulations of peat swamps (Doktor and Gradziński, 1985, 1999). Observed palaeosols form thin and simple profiles, consisting of the poorly altered, basal C horizon, followed by usually one mineral B-horizon, commonly thinly developed, and containing pedogenic structures. The mineral soils are overlain directly by a Histosol, preserved as an organic H-horizon, represented by a coal seam (Figs 3 and S1). C-horizons were often rooted and consisted of massive mudstone to fine-grained sandstone, with common

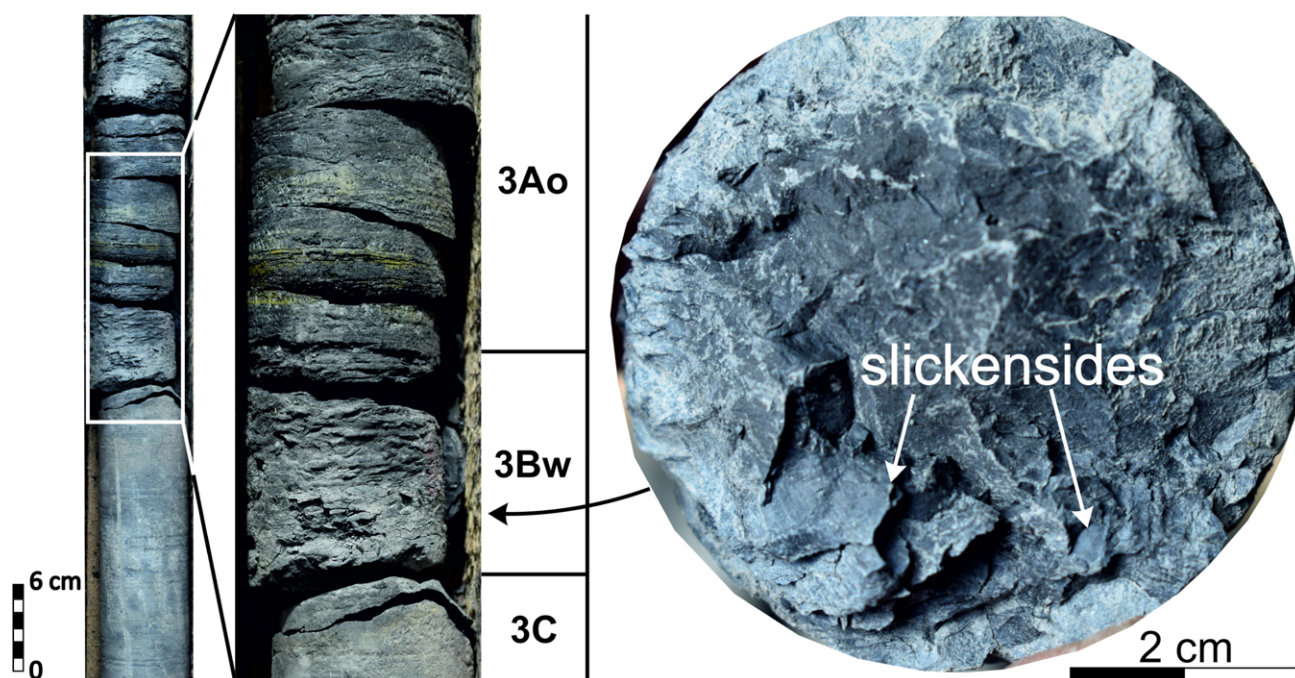


Fig. 3. Lower part of the compound gleyed vertic Protosol from the WPTX core depth 965.7 m with a sharply bounded and thinly developed Bw horizon and sparse slickensides.

bioturbation and siderite cement. The grey to dark grey mudstone to muddy siltstone occurring above represented B-horizons that were 5–40 cm thick. B-horizons most commonly contained organic roots, fine bioturbations, and scattered slickensides (Bw horizon; Fig. 3). Fine siderite nodules and slickensides, accompanied by a weak, medium to fine, wedge-shaped aggregate or an angular, blocky structure, were present, though rare, in some horizons (Bssg horizon). The oxidation of siderite concentrations led to the formation of fine to medium, orange-brown iron oxide mottles in some horizons. Siderite concentrations occurred as diffuse cements or fine- to medium-sized nodules, dispersed in a muddy matrix, or formed an indurated siderite-cemented horizon at the base of the palaeosol profile (Bg horizon). Palaeosols form typically simple profiles, with only one mineral B-horizon. Several vertically stacked B-horizons of variable maturity and/or slightly different composition were rare, as well as compound palaeosol sections, with up to three vertically stacked palaeosol profiles (Fig. 3).

Weak development of pedogenic structures, poor horizonation of palaeosol profiles, and the common occurrence of organic material in the form of roots and fine plant debris, together with the presence of siderite cements and concentrations/nodules, allowed the observed palaeosol profiles to be classified as gleyed Protosols (Mack *et al.*, 1993). Slickensides and weak, wedge-shaped or angular, blocky structures indicated periods of repeated shrinking and swelling of the palaeosol matrix. The oxidation of organic matter and iron in siderite, manifested as mottling, suggest fluctuation of the water table.

Micromorphology

Most samples had homogeneous material, i.e., showed no well-defined ped structures or bioturbations. The latter

was distinguishable, for instance, in sample W966.5 that displayed deformed burrows (Fig. 4). Furthermore, some samples still preserved the original lamination (J550.9, J663.5, W1087.7, AM1458.0, AP845.5, AP992.4, AP996.0, AP1398.4, AP1010.2, G243.9, and G294.1). Notably, only samples W1087.7, AM1458.0, AP1398.4 showed macroscopic lamination as well. Well-developed microped structure was observed in samples ZOR525.6, ZOR525.3, ZOR530.9, G226.1, and G243.9 (Fig. 5). Well-developed parallel-striated b-fabric was visible in samples AP845.5, AP992.4, AP996.0, AP1398.4, AP1010.2, ZOR525.3, ZOR530.9, G243.9, G294.1, and G297.6. The fabric was not always visible in an entire thin section. Samples AM1458.0, AP845.5, Z530.9, and G297.6 displayed clay skins along voids or cracks, which indicates clay illuviation. Organic matter was present as roots, small accumulations of particulate organic material, or irregular patches in most of the samples, and was particularly abundant in samples W966.5, W1087.7, and AP1010.2. Furthermore, in samples AM1457.1, AP992.4, AP966.0, and G294.1, macerals, probably liptinite, could be observed. Samples AP992.4 and AP966.0 additionally had coal bands. Cracks and void-related features were widespread. Siderite was present as small (mm-scale) spheroidal crystals or accumulations (samples W966.6, AP845.5, AP1010.2, AM1458.0, ZOR525.6). A large accumulation was noticed in sample W966.6. Dispersed iron oxides were observed in sample G243.9.

Scanning Electron Microscopy

SEM images showed that kaolinite locally develops characteristic booklet-like aggregates, as exemplified by sample J663.5 (Fig. 6A). SEM-EDS analyses also revealed well-preserved pedogenic fractures within the rocks (Fig. 6B). Another authigenic mineral that is quite common in the

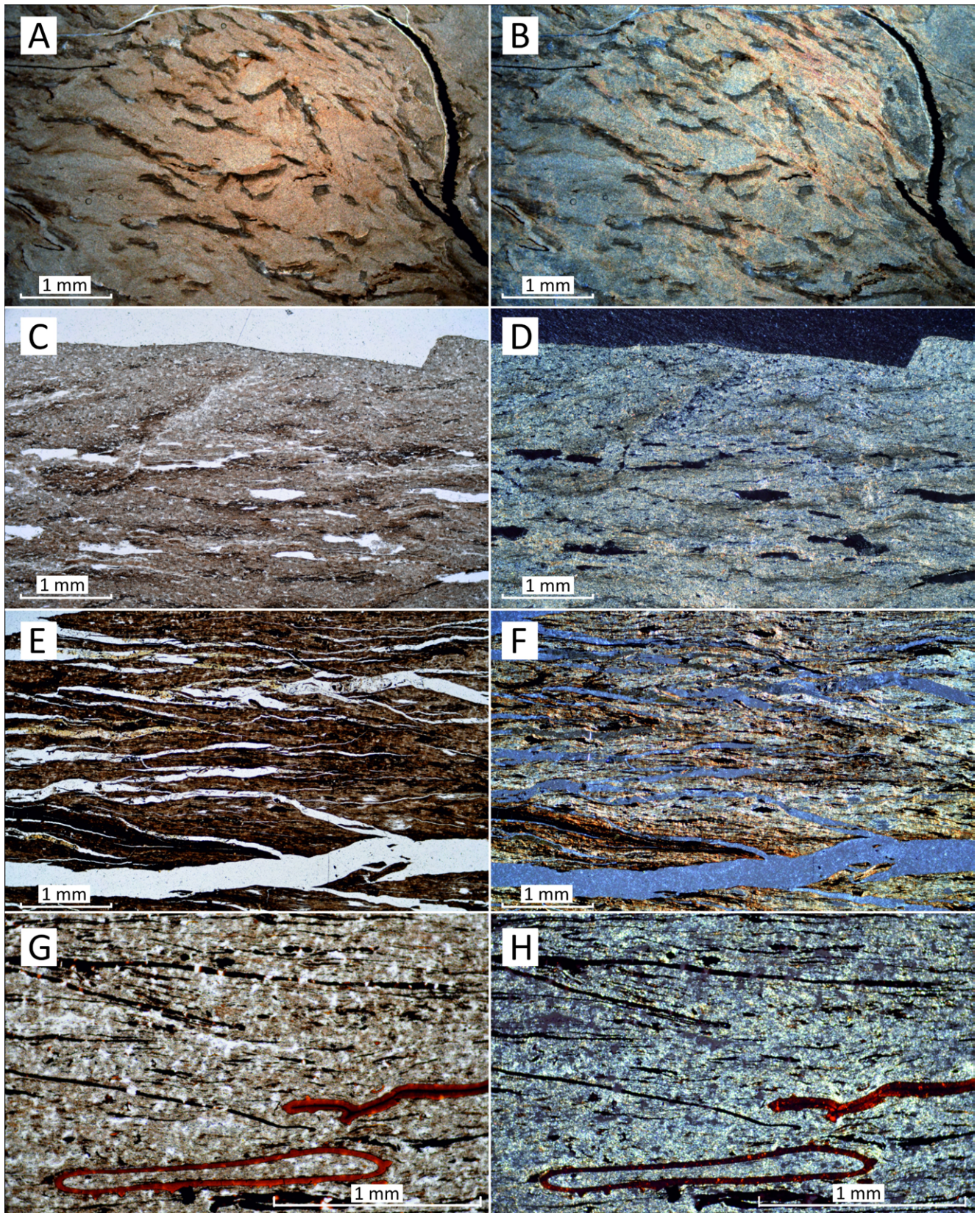


Fig. 4. Micromorphology of the studied palaeosol samples. **A, B.** Burrows deformed by pedogenic processes (e.g., rooting, shrinking and swelling; W966.5). **C, D.** Relic lamination with thin burrows AM1458.0. **E, F.** Relic lamination? AP992.4. **G, H.** Rooted mudstone with liptinite macerals at lower part, AP966.0. **A, C, E, G.** – plain light; **B, D, F, H** – polarized light.

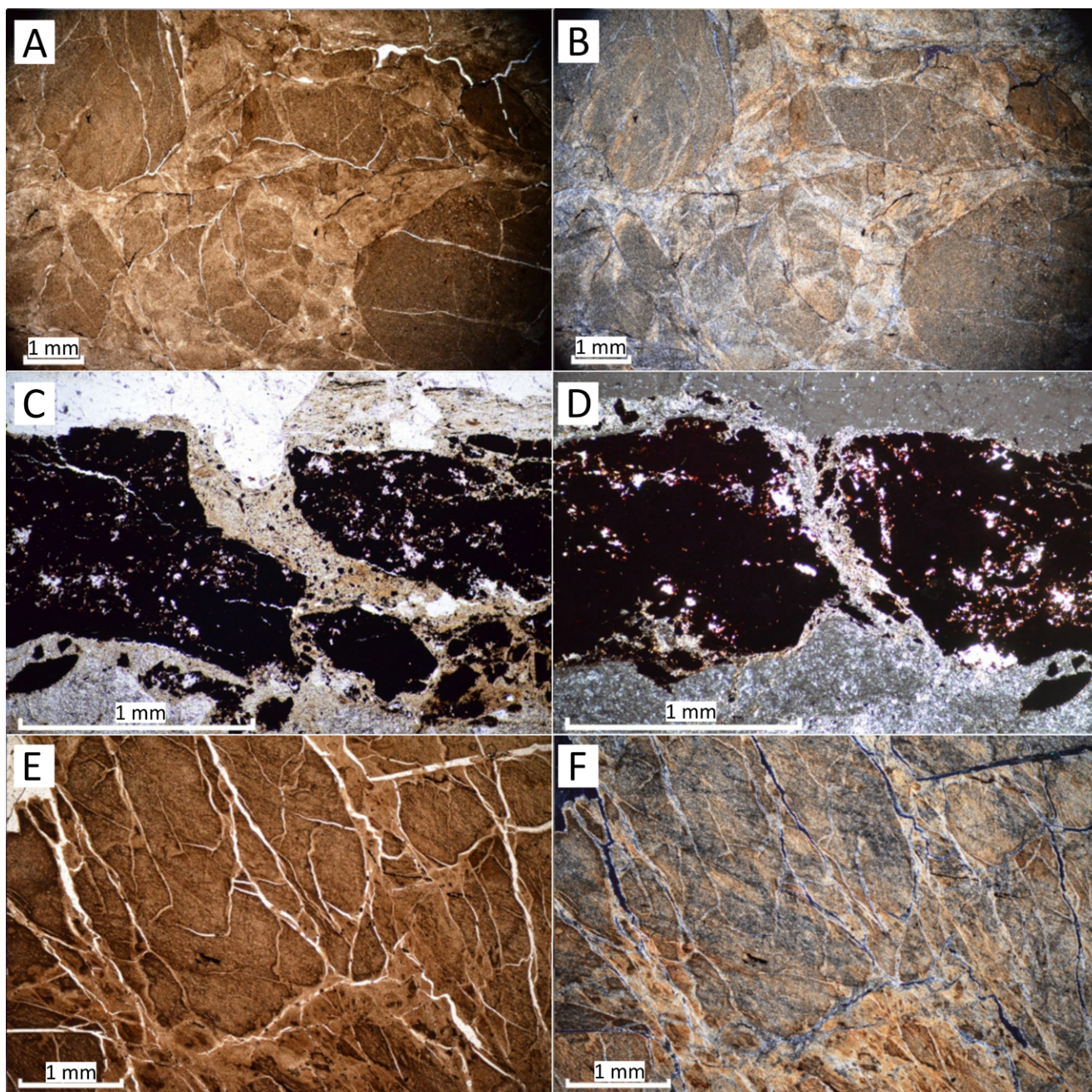


Fig. 5. Micromorphology of the studied palaeosol samples. **A, B.** Well-developed micropedal structure shows large peds, divided by zones of crushed ped debris, possibly filling an original crack system, ZOR525.3. **C, D.** Fine crack, filled by randomly oriented clays, ZOR530.9. **E, F.** Well-developed, plane-parallel birefringence fabric and micropedal structure, defined by a dense network of slickensides, partly covered by clay accumulations – G243.9. **A, C, E** – plain light; **B, D, F** – polarized light.

palaeosol samples studied is siderite (Fig. 6C). In several places, it occurs as well-developed, automorphic crystal forms, indicating *in situ* growth during pedogenesis and early diagenesis, under locally reducing conditions. Early diagenetic growth is further evidenced by the bending of the clay-mineral laminae surrounding the crystals, showing that siderite formed *in situ* and displaced the adjacent fabric. In some areas, the crystals coalesce into larger aggregates (Fig. 6C). Its composition is variable, particularly with respect to magnesium, which locally reaches up to 7 wt.% and often produces distinct compositional zoning, with the outer rims of some crystals enriched in Mg (Fig. 6D). These features

emphasize the authigenic origin of the siderite and reflect subtle shifts in pore-water chemistry and changing geochemical conditions during pedogenic processes and early burial. The accessory mineral assemblage in the palaeosols studied here consists of galena (Fig. 7A), pyrite (Fig. 7B), sphalerite (Fig. 7C), framboidal pyrite (Fig. 7D), chalcocopyrite, barite (Fig. 7E), apatite, and goethite (Fig. 7F). Most of them are associated with organic matter, e.g., galena, sphalerite, pyrite; while others occur as fillings of the fractures formed after the decay of roots, e.g., galena, barite. Some of the pyrite anhedral crystals contain as much as 3 wt.% As.

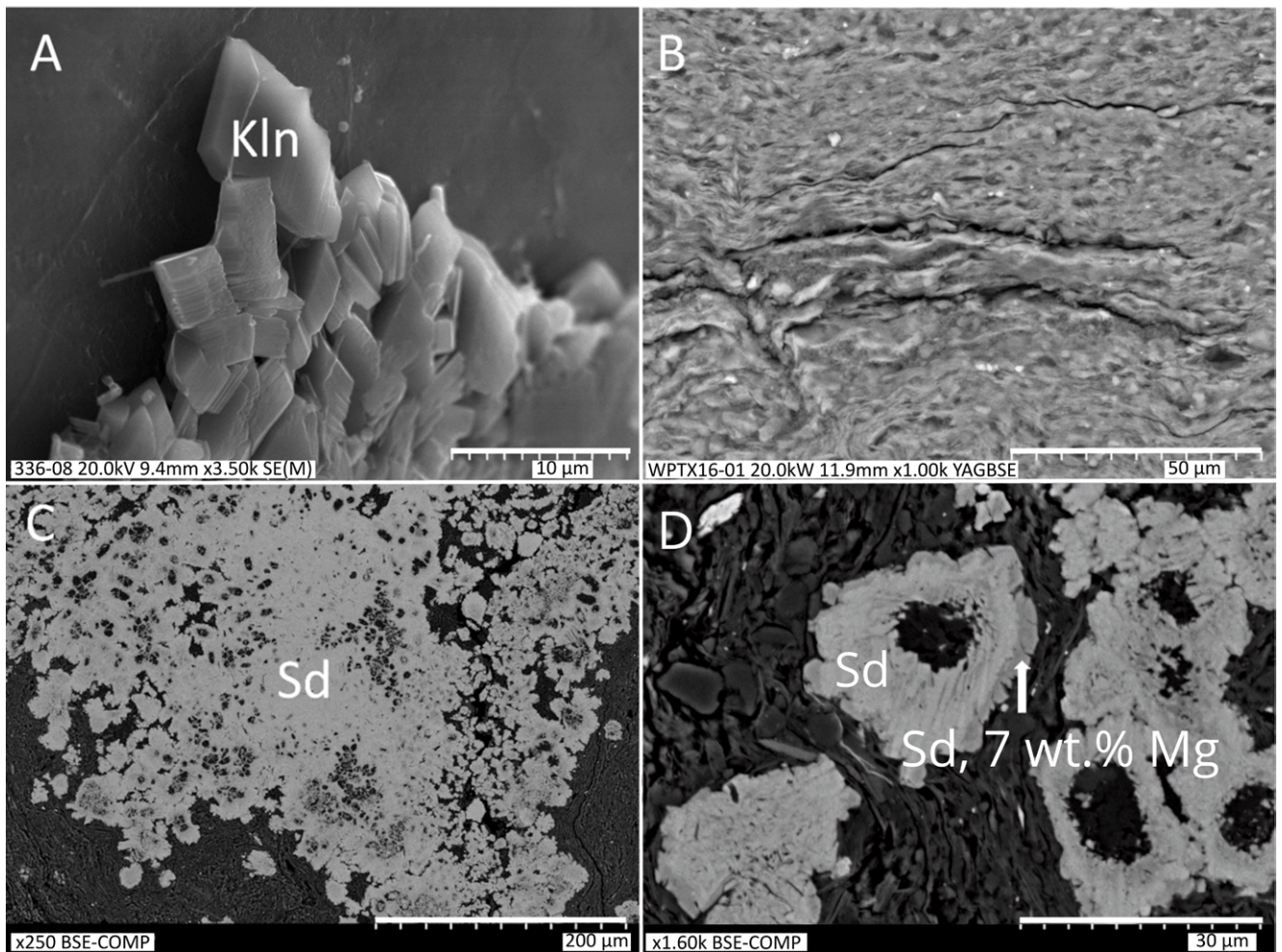


Fig. 6. Scanning Electron Microscopy (SEM) images. **A.** Sample J663.5 with kaolinite booklets. **B.** Sample W966.5 with pedogenic cracks. **C.** Sample API010.2 with aggregate of authigenic siderite. **D.** Zonation of siderite crystals, with up to 7 wt.% of Mg as determined by the SEM-EDS analysis (sample API010.2).. Kln – kaolinite, Sd – siderite.

Chemical composition

No clear trends in chemical composition were discernible with regard to geographic location or sample depth. The SiO_2 content varied between 38.62 and 68.23 wt.%, and Al_2O_3 between 14.22 and 27.17 wt.% (Tab. 2). The lowest total Fe concentration of 1.09 wt.% was measured for the G297.6 sample, and the largest was equal to 17.21 wt.% for the ZOR524.8 sample. The total Fe contents were highly variable, with the ZOR524.8 sample being an outlier. The concentrations of CaO and MgO were in the range from 0.04 to 1.39 wt.% and from 0.45 to 3.88 wt.%, respectively, while those of K_2O and Na_2O were between 1.55 and 5.90 and between 0.22 and 0.58 wt.%, respectively (Tab. 2).

The geochemical weathering indices generally showed very limited variability (Fig. 8). CIW was >90 for all samples except the AP992.4 sample, which had a CIW value of 87. The sample ZOR524.8 had the lowest CALMAG value of 62, while the remaining samples generally had CALMAG values between 83 and 94. The Ruxton ratios were relatively constant, ranging from 3 to 4.5 for the majority of the samples. The Ruxton ratio indicates poor leaching of clay particles in immature palaeosol profiles (Basilici

et al., 2016). The $\text{TiO}_2/\text{Al}_2\text{O}_3$ ratio, ranging from 0.03 to 0.04 (excluding samples W840.3 and ZOR1510.1 that had anomalously high $\text{TiO}_2/\text{Al}_2\text{O}_3$ ratios), indicated relatively constant mobility of Al in the investigated sample set. Base loss showed the largest relative changes, ranging from 5.1 to 16.3, with the maximum in the AP992.4 sample. The ω - ψ metrics (Fig. 9) indicated that most samples were moderately to highly weathered, compared to the model Toorongu weathering profile, used to construct the ω - ψ approach (Lipp *et al.*, 2020). All but two samples plotted in the felsic field. The outliers were sample AP992.4, which had elevated Ca, and ZOR524.6, which had an elevated Fe content, due to a high amount of pedogenic siderite. No correlations between both metrics (i.e., ψ and ω) and sample depth were detected. The examination of the Mafic-Felsic-RW ternary diagram led to conclusions similar to those of the ω – ψ approach (Fig. 10). All samples plot in the felsic field and close to the RW apex, indicating a high degree of weathering. In this approach, greater variability in the weathering component for samples from the APOR, WPTX, and ZOR boreholes was observed than in other approaches, such as CIA-K or CALMAG (Fig. 8).

The values of the Rb/Sr ratio varied from 0.67 to 3.09, of the Sr/Cu ratio from 1.80 to 4.96, and of the Sr/Ba ratio from 0.16 to 0.44 (Fig. 11). The Sr/Ba and Sr/Cu ratios were low (<0.3 and <4.0, for most of the samples, respectively). The La content in the studied palaeosols ranged from 5.9 ppm to 56.3 ppm, and the Th content from 3.3 ppm to 25.9 ppm.

The La/Th ratio varied in the range of 1.42–2.92, with just one sample (J516.2) exceeding the threshold value of 2.80. Obtained values for Mo were < 5 ppm (Table 2). The V/Cr ratios of the examined samples were below 2. The Th/U ratios were between 0.66 and 6.14, with an average of 2.69 (Fig. 11).

Table 2

Chemical composition of the bulk palaeosol samples (in wt.%).

Sample	SiO ₂	Al ₂ O ₃	CaO	Fe ₂ O ₃	K ₂ O	MgO	Na ₂ O	P ₂ O ₅	TiO ₂	LOI
AM1457.1	53.96	23.72	0.13	3.45	3.42	1.09	0.58	0.09	0.56	12.3
AM1458.0	54.61	24.69	0.08	2.13	3.69	1.09	0.47	0.07	0.60	10.4
AP842.8	50.01	22.04	0.13	5.40	3.26	1.46	0.42	0.07	0.53	16.2
AP845.5	55.14	19.59	0.10	4.15	3.73	1.23	0.44	0.09	0.61	9.9
AP992.4	38.62	21.27	1.39	2.37	2.66	1.44	0.39	0.12	0.47	29.0
AP996.0	39.51	18.79	0.13	2.39	2.46	0.99	0.33	0.12	0.42	33.1
AP1010.2	49.09	23.06	0.08	2.92	3.61	1.13	0.55	0.07	0.54	17.9
AP1398.4	49.97	23.50	0.07	1.44	3.57	0.76	0.58	0.07	0.57	14.4
G226.1	54.69	27.05	0.14	1.49	3.26	0.85	0.28	0.03	0.65	11.1
G243.9	50.54	25.27	0.22	6.22	3.22	1.44	0.29	0.08	0.57	11.6
G286.1	47.79	23.67	0.24	10.14	3.35	1.76	0.26	0.07	0.57	12.1
G294.1	50.32	22.23	0.11	2.83	4.08	0.78	0.34	0.06	0.64	12.2
G297.6	60.65	17.93	0.06	1.09	3.10	0.45	0.26	0.04	0.67	8.5
J498.3	57.76	24.54	0.07	2.56	3.06	1.18	0.32	0.06	0.64	9.9
J502.2	54.93	19.76	0.04	3.73	3.61	1.39	0.36	0.05	0.63	10.6
J502.4	68.23	17.06	0.04	2.54	2.48	1.04	0.22	0.03	0.51	6.9
J508.8	51.07	24.54	0.17	5.98	3.51	1.44	0.41	0.08	0.58	11.0
J511.7	44.04	14.22	0.08	1.66	1.92	0.73	0.25	0.03	0.41	36.2
J512.0	57.88	21.42	0.06	3.77	3.46	1.44	0.35	0.04	0.62	8.5
J516.2	51.31	23.82	0.10	3.53	3.59	1.53	0.40	0.07	0.57	14.3
J536.4	55.66	22.99	0.06	3.14	3.18	1.33	0.37	0.05	0.64	9.4
J541.6	53.13	19.95	0.04	2.90	3.47	0.90	0.43	0.06	0.64	10.8
J550.9	54.64	19.40	0.04	2.27	3.46	0.80	0.45	0.06	0.64	10.1
J551.8	59.79	19.80	0.06	2.10	3.20	0.90	0.34	0.05	0.65	8.9
J593.8	47.20	23.46	0.27	11.01	3.48	1.26	0.45	0.16	0.49	12.1
J623.6	57.74	19.34	0.04	2.60	3.42	1.06	0.38	0.04	0.67	9.7
J634.5	50.85	25.84	0.07	1.56	1.55	0.73	0.46	0.04	0.67	16.0
J663.5	56.03	21.63	0.07	2.63	3.14	1.13	0.44	0.04	0.57	13.7
W840.3	53.71	25.37	0.16	2.1	4.01	1.16	0.47	1.01	7.91	11.6
W966.5	56.72	22.91	0.10	2.37	3.25	0.99	0.48	0.08	0.60	11.9
W966.6	58.35	24.74	0.10	2.52	3.65	1.09	0.46	0.09	0.65	8.9
W1087.7	54.57	24.88	0.07	2.29	4.25	1.04	0.53	0.05	0.60	11.0
ZOR524.8	38.86	17.98	0.73	17.21	2.7	3.88	0.32	0.72	2.25	17.1
ZOR525.3	52.76	27.17	0.16	2.87	3.97	1.47	0.43	1.06	3.47	9.7
ZOR525.6	55.31	24.44	0.10	3.79	3.75	1.49	0.46	0.08	0.62	9.1
ZOR530.9	48.89	24.48	0.11	2.14	3.40	1.13	0.49	0.07	0.58	18.3
ZOR1361.7	49.11	26.77	0.48	2.06	3.13	0.93	0.44	0.38	0.60	15.0
ZOR1510.1	54.95	24.39	0.14	2.66	5.9	1.26	0.25	1.03	5.38	9.0

Mineralogy

The mineral composition of bulk samples was dominated by phyllosilicates (Fig. 12). Kaolinite and mixed-layer illite-smectite (Ill-Sme) were the most abundant minerals, each with an average content of close to 25%. Muscovite and quartz were also quite abundant, each with an average content of 21%. There were no statistically significant

differences in mineral content among the boreholes for phases with an average content >5%, with two exceptions. Muscovite content was lower in the JAW5109 borehole than in the APOR borehole, and the kaolinite content was statistically significantly greater in JAW5109 than in the WP TXA borehole, as evidenced by the results of the Kruskal-Wallis test, followed by the post-hoc Dunn's test. Feldspars (both K-feldspars and plagioclases), carbonates, anatase, and chlorite were present only in some samples (Fig. 12).

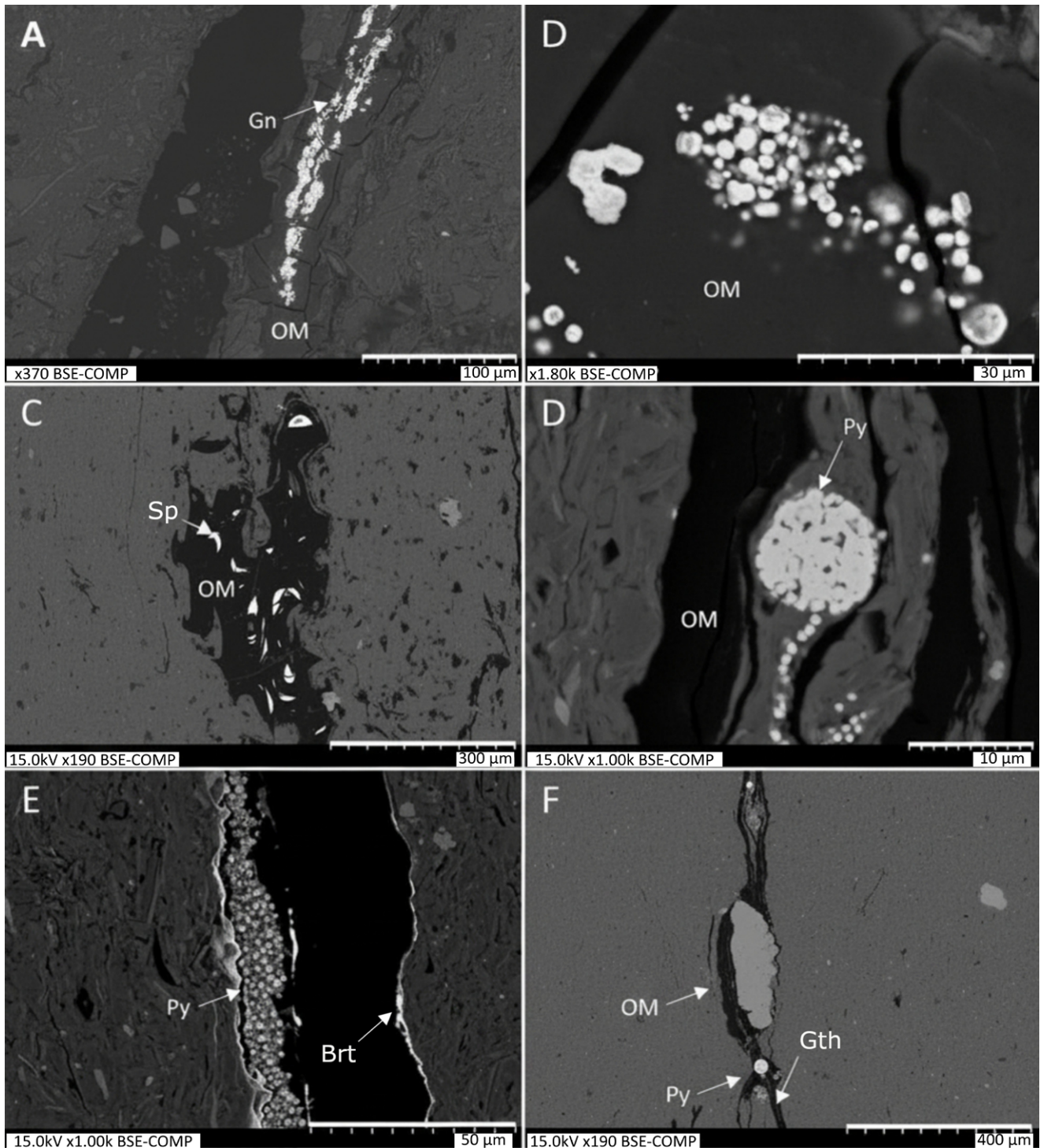


Fig. 7. SEM images. **A.** The crystallization of galena with the root fossil and arsenic-bearing pyrite (up to 3 wt.% As), associated with organic matter as seen in (**B**, **C**) spherulitic pyrite associated with organic matter. **D.** Framboidal pyrite, associated with organic matter. **E.** A fracture, filled with barite and pyrite. **F.** Apatite, goethite, and framboidal pyrite, associated with organic matter. **A**, **B** – sample G286.1; **C**, **D**, **E**, **F** – sample ZOR1361.7; **Ap** – apatite, **Brt** – barite, **Gn** – galena, **Gth** – goethite, **OM** – organic matter, **Py** – pyrite, **Sp** – spherulite.

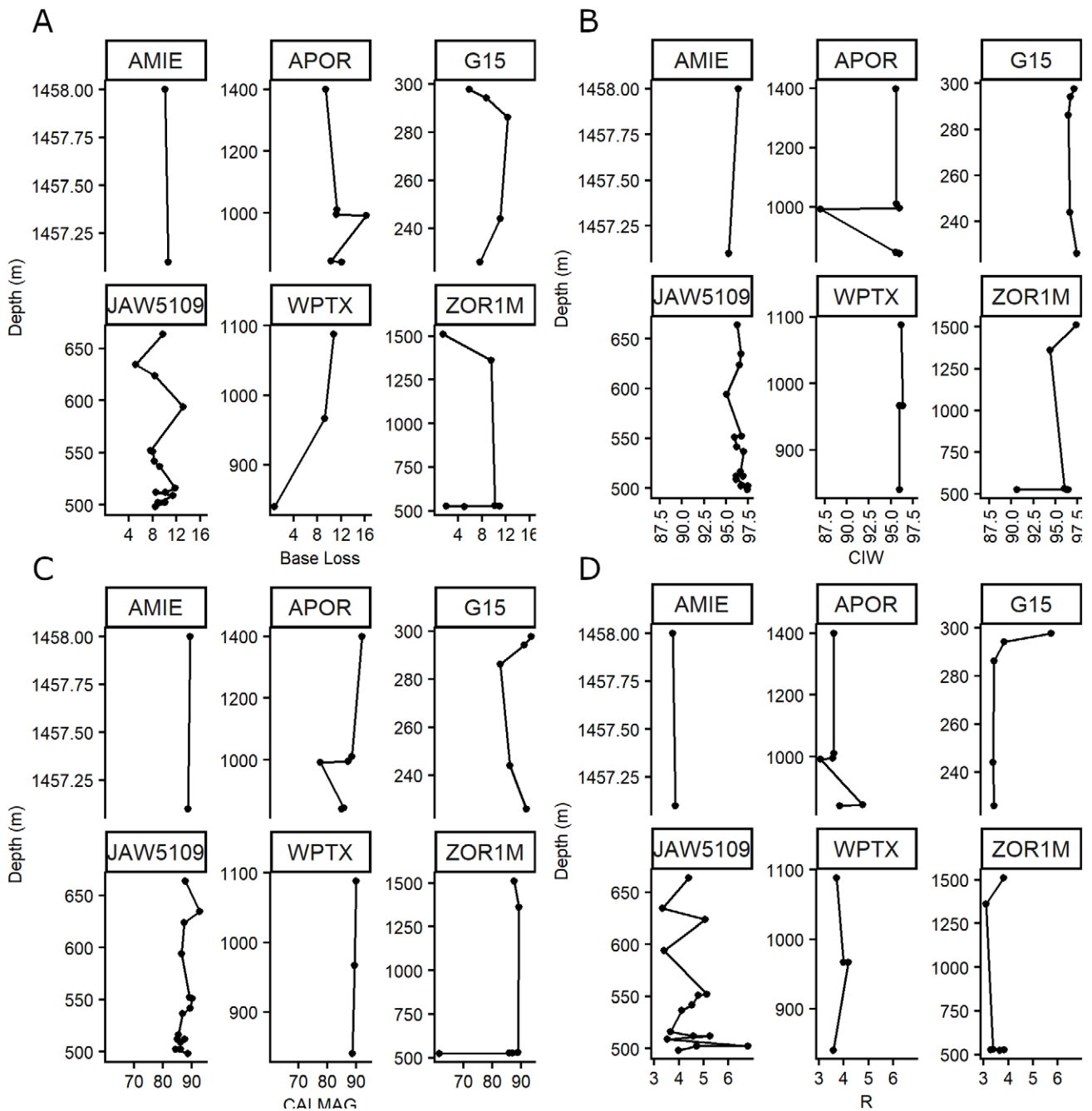


Fig. 8. Selected geochemical weathering indices for the investigated samples. CIW – Chemical Index of Weathering (Harnois, 1988); CALMAG – Calcium-Magnesium Weathering Index (Nordt and Driese, 2010); Base Loss (Sheldon and Tabor, 2009); Clayeyness (Ruxton, 1968).

The mineral composition of the $< 2 \mu\text{m}$ size fraction, separated from the palaeosol samples, showed small variability in the qualitative composition of the clay mineral assemblage. The clay minerals in this size fraction were identified, on the basis of the criteria provided by Śródoń (2013). All samples contained dioctahedral mica (“muscovite”), kaolinite, and Ill-Sme. Chlorite was present in all samples, except for AP1398.4, Z524.8, and G226.1, and all samples from the WPTX borehole. Small quartz impurities were present in the samples from the JAW5109, WP TXA, and AMIE boreholes. Generally, there were no trends in the relative clay mineral contents with depth for a given borehole,

as was evidenced by the changes in the relative peak areas in the XRD patterns, with a couple of exceptions (Fig. 13 and Supplementary data available at the IGS PAS Data Portal). The Ill-Sme and kaolinite contents increased relative to muscovite and chlorite with depth in the JAW5109 borehole. In the WP TXA borehole, muscovite and kaolinite contents were the greatest in the W996.5 sample. Chlorite and kaolinite contents were elevated in the shallower samples from the APOR borehole, and the same part of the borehole seemed to have more smectitic Ill-Sme, with the latter observed again in the ZOR1M borehole.

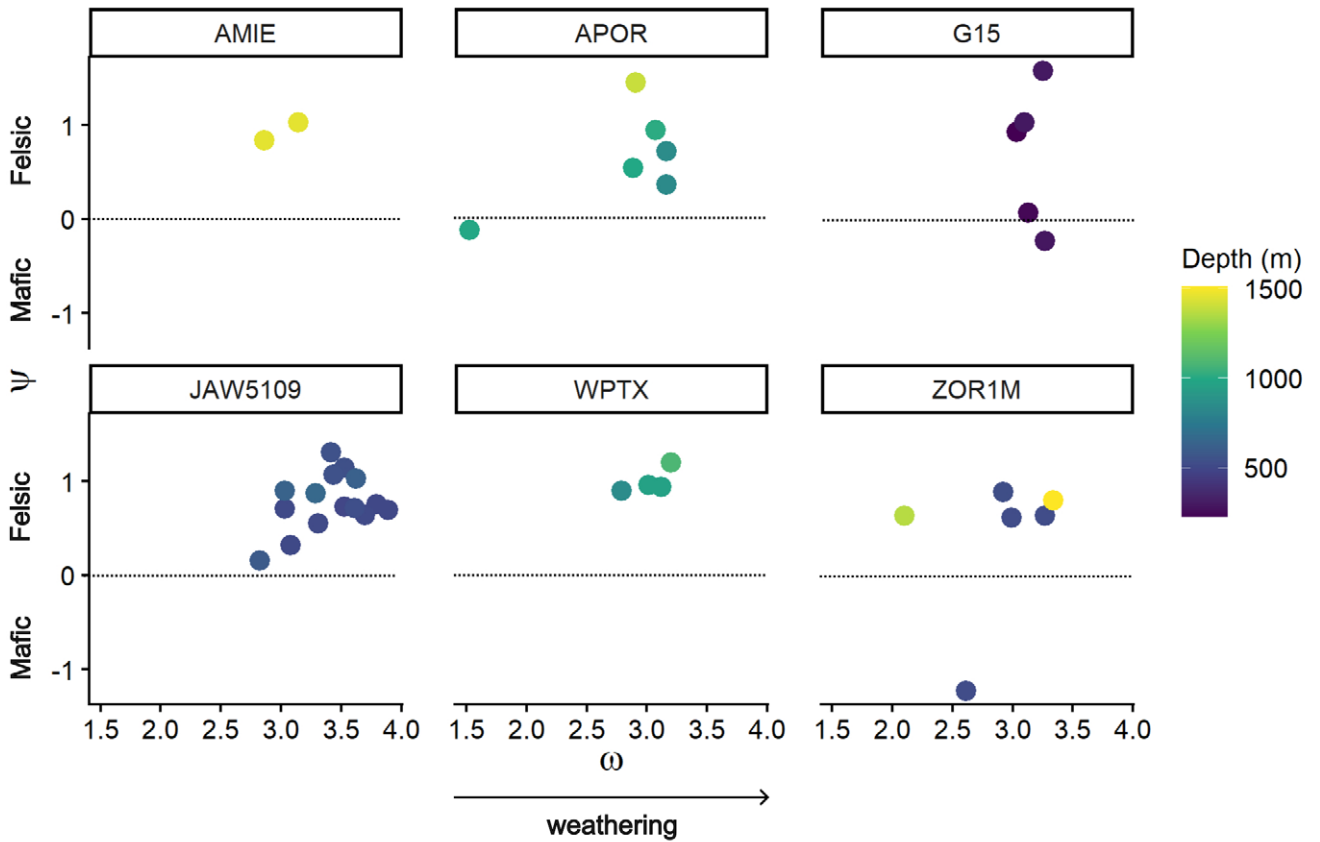


Fig. 9. The ω - ψ plot (Lipp *et al.*, 2020) for the investigated samples. Positive ψ values indicate that the parent material was felsic. Sample AP992.4 plots in the mafic field, due to elevated Ca, and ZOR524.8, due to high siderite content. The ω values > 2 indicate that the material was moderately to highly weathered, compared to the model Torongoo weathering profile of Lipp *et al.* (2020).

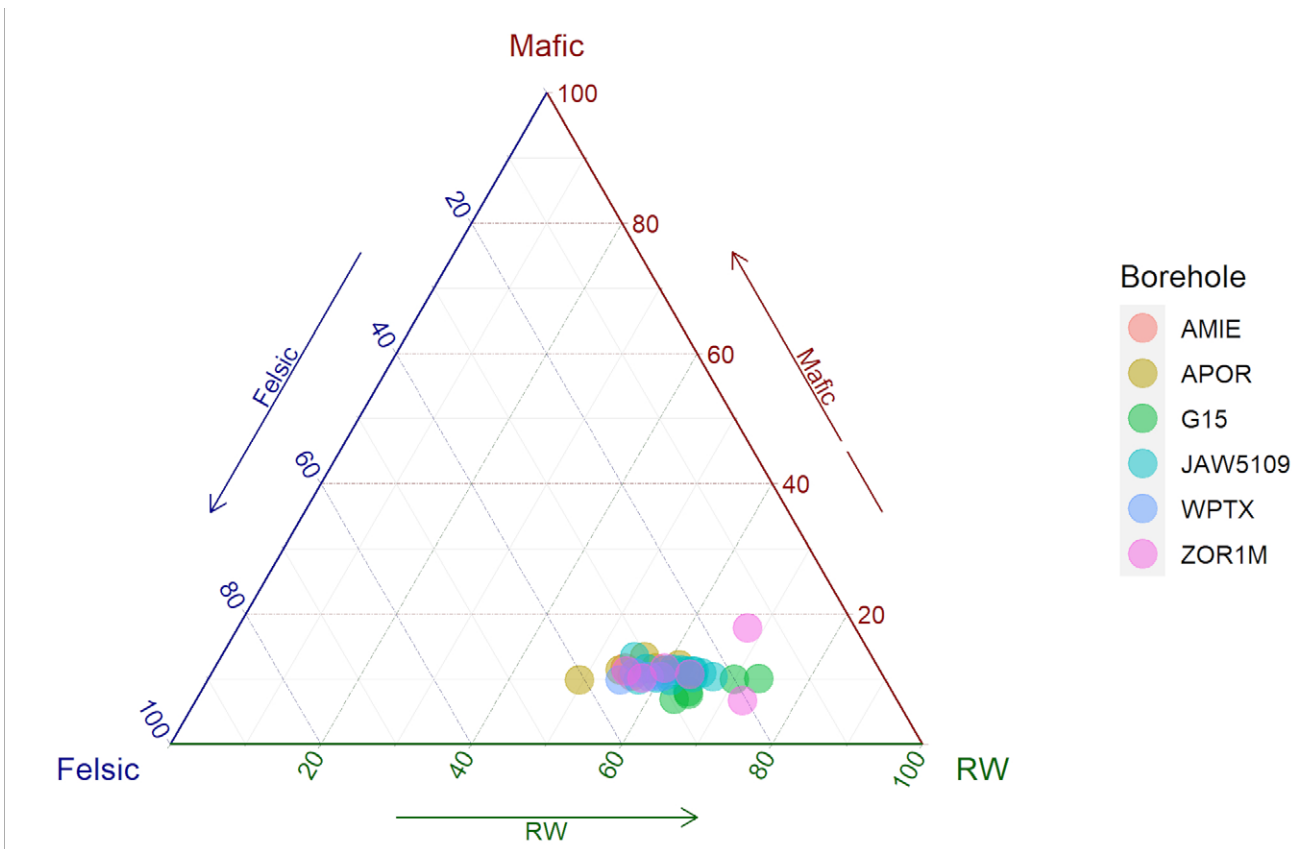


Fig. 10. Mafic-Felsic-RW plots ternary diagrams, calculated following Cho and Ohta (2022).

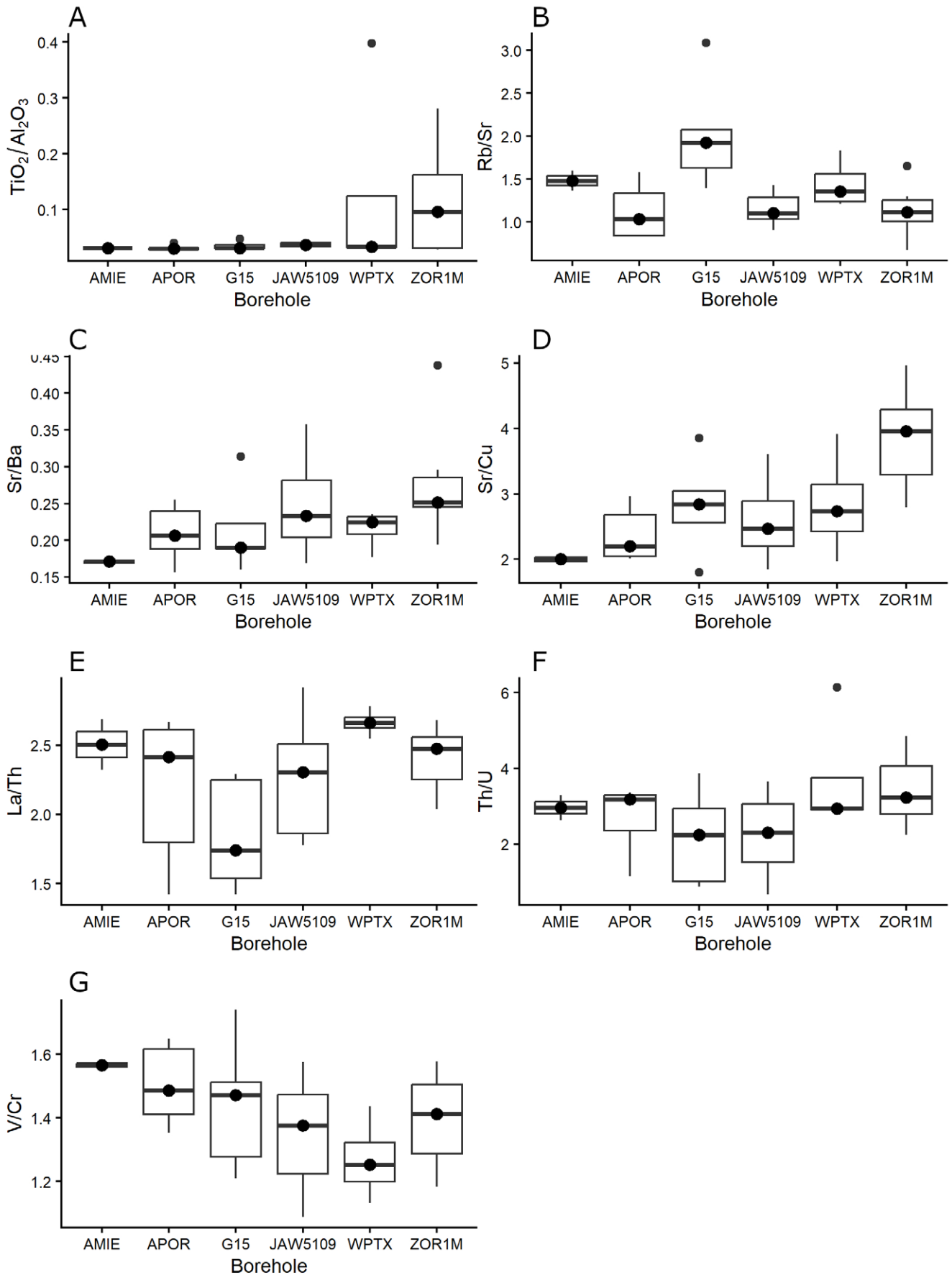


Fig. 11. Box plots of selected elemental ratios for the samples investigated.

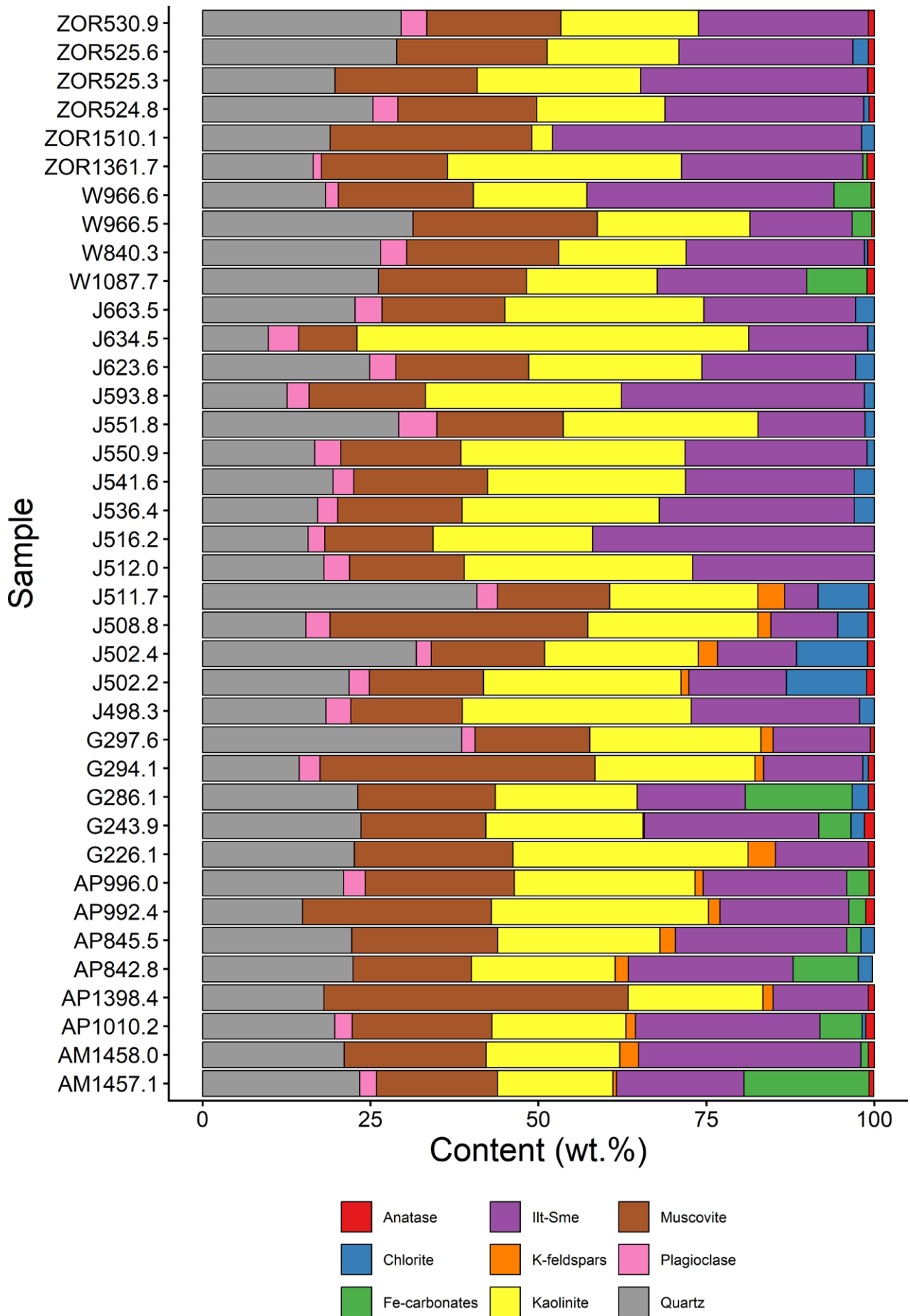


Fig. 12. Mineralogical composition (in wt.%) of bulk palaeosol samples, based on the quantitative X-Ray diffractometry (QXRD).

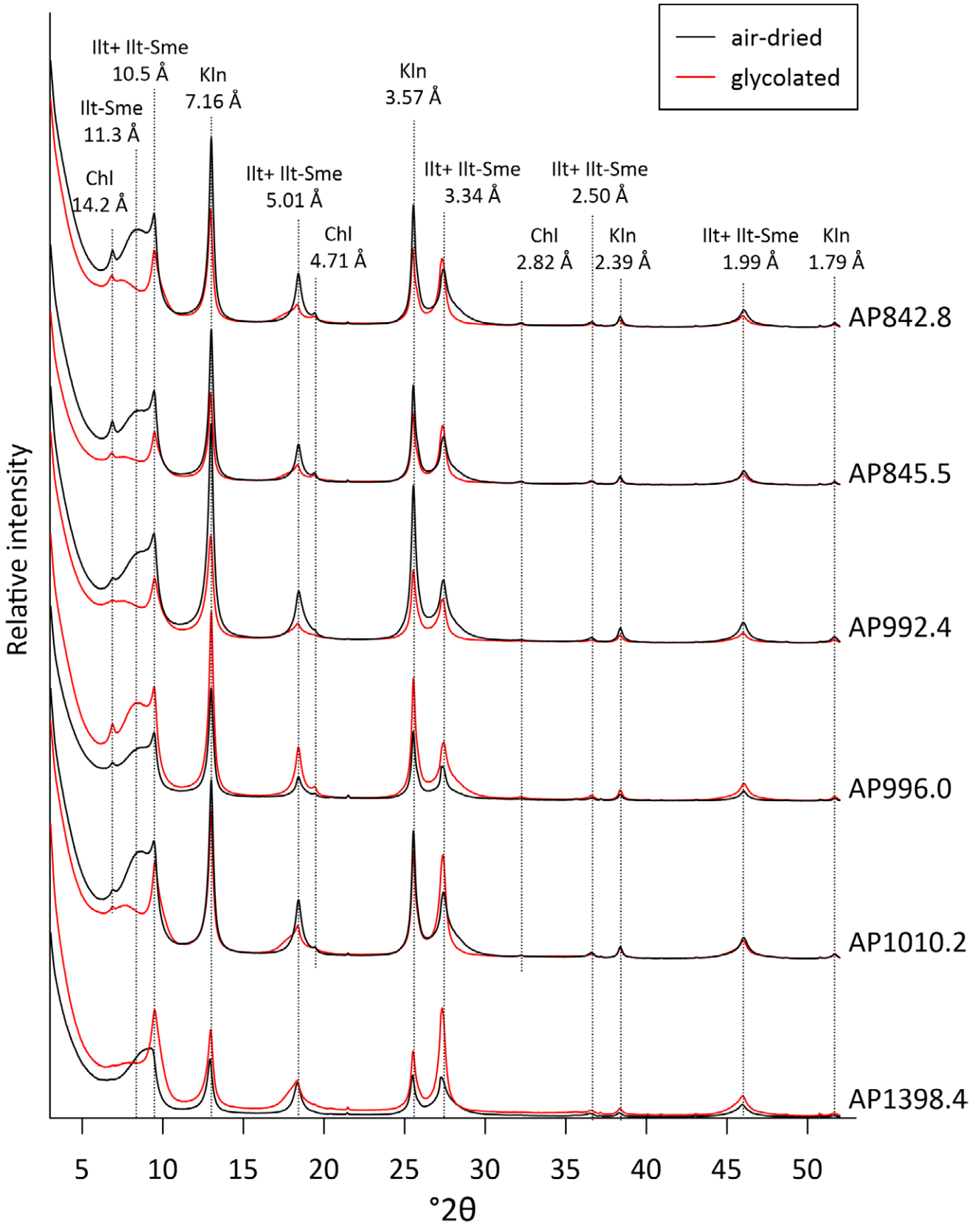


Fig. 13. XRD patterns of oriented specimens of Ca^{2+} -saturated $< 2 \mu\text{m}$ size fraction of samples from the APOR1 borehole in air-dried and glycolated state. XRD patterns of the remaining samples are provided in the Supplementary Data available online at IGS PAS Data Portal. Chl – chlorite, Illt – illite, Illt-Sme – illite-smectite, Kln – kaolinite.

DISCUSSION

The applicability of different proxies to the estimation of palaeosol maturity

One can attempt to assess the maturity of palaeosols investigated on the basis of 1) micromorphology, 2) geochemistry, and 3) mineralogy. Micromorphological analysis was the most helpful method for identifying more and less mature palaeosols. It also allowed for identifying the primary (sedimentological, not altered), pedogenic and post-burial features of the material. Preservation of lamination in many of the samples investigated indicates only very limited pedogenesis. Therefore, samples with lamination preserved are interpreted here as being highly immature (Protosols), since root fragments are the only pedogenic feature observed in these samples. In some samples, the lamination was still visible, despite the occurrence of roots perpendicular to it. A massive, micromorphological soil structure, without cracks and other pedogenic features, suggests low activity of pedogenic processes, which the sample W966.6 exemplifies. On the other hand, the presence of material with various grain sizes and the presence of cracks, filled with material clearly different from the surrounding soil, as well as accumulations of soil aggregates, indicate great activity of pedogenetic processes and higher palaeosol maturity. In samples AM1457.1, AM1458.0, and G226.1, lenticular structures, filled with materials, may be the remnants of soil pores, deformed by compaction. The occurrence of clay skins (sample Z530.9) indicates clay illuviation. Nevertheless, none of the aforementioned processes lead to the pronounced development of features that allow the classification of palaeosols, other than Protosols.

The mineralogical composition was less helpful in identifying the maturity of palaeosol horizons than micromorphological analysis. The main difficulty stemmed from the fact that the analyzed material contained phases from different sources: 1) detrital phases from the parent material, 2) pedogenic phases, and 3) diagenetic phases. Quartz, coarse dioctahedral mica, and feldspars belong to the first group. The origin of kaolinite and Ill-Sme is somewhat ambiguous because, by analogy with present-day weathering systems (Bayon *et al.*, 2015), these minerals may have been present in the suspended sediment, deposited by Carboniferous rivers. Kaolinite and Ill-Sme are, at the same time, common pedogenic minerals (Churchman and Lowe, 2012) and might also be formed during diagenetic processes (Eberl, 1984; Nadeau, 1998). The presence of kaolinite booklets indicates their formation *in situ* or after brief transport; therefore, at least a part of kaolinite is pedogenic or/and diagenetic. At least some part of Ill-Sme is also diagenetic, due to the Triassic K-metasomatism episode in the USB basin (Środoń *et al.*, 2006). Chlorite most likely originated from the parent material. Its diagenetic formation is considered unlikely, as temperatures were insufficient for chlorite formation. Carbonates in the material investigated were mostly represented by diagenetic siderite. Diagenetic features of siderite, such as large and well-developed sizes, and also observed under CPL, are visible in the thin sections of samples W966.6 and AM1458.0.

The analyzed palaeosols showed relatively small variability in the composition of their bulk and <2 µm size

fraction, with most of the observed variability coming from the outliers (Fig. 12). Such small variability means that the rivers supplied similar material in all of the locations investigated, indicating a uniform source of alimentation and relatively constant flow conditions. It also means that the diagenetic history of samples from different boreholes did not vary much, which is in agreement with what is known about the diagenetic history of the area (Środoń *et al.*, 2006; Botor, 2020). The low content of minerals susceptible to weathering, such as plagioclases and chlorite, should not be misinterpreted as high palaeosol maturity in the samples investigated. First of all, the parent material of the transported materials is not known, these minerals might have not been present in it from the beginning, these phases might have been removed by weathering in the other part of the catchments, before redeposition to the present location, or might have been removed from by sorting during fluvial transport. Secondly, the micromorphological features of the samples indicate a generally low maturity of the palaeosols investigated. Late Carboniferous pedogenesis was definitely not the process that determined the mineralogical composition of the samples investigated. The latter is even more evident if one considers the values of various geochemical weathering proxies, calculated for the samples investigated (Fig. 8). The CIW ratios are very high (>90), indicating advanced weathering. The same applies to CALMAG. Trace geochemical proxies (Rb/Sr, Sr/Ba, and Sr/Cu ratios) and the TiO₂/Al₂O₃ ratio also indicate that the material investigated had undergone intensive weathering in a warm and humid climate (Jia *et al.*, 2013; Tao *et al.*, 2017), in agreement with the postulated near-equatorial position of the USB during the Pennsylvanian (Opluštil *et al.*, 2019, 2024). Taken at face value, these proxies indicate high maturity of the material, which implies advanced pedogenesis. Such an interpretation, however, cannot be reconciled with the observed macro- and microscopic features, unequivocally indicating weak pedogenesis in most of the samples. This means that the material was already highly weathered when finally deposited on the alluvial floodplain, where it was only weakly modified by pedogenesis before burial. Therefore, the geochemical and mineralogical compositions reflect weathering that had occurred before the material was redeposited by fluvial transport. Such a situation appears to be common in fluvial settings, as it was also identified by Jewuła *et al.* (2026) for the Jurassic coal-bearing strata of the Reșița Basin (Romania). These authors also reported highly mature mineralogical compositions of weakly developed alluvial palaeosols. Such findings support the conclusion that geochemical weathering proxies should not be considered as indicative of advanced *in situ* weathering in alluvial settings, as they likely are biased by sorting during fluvial transport.

Palaeosols of the Mudstone Series as palaeoenvironment archives

The MS was deposited by low-energy, meandering fluvial systems, dominated by fine-grained, off-channel sedimentation (Doktor and Gradziński, 1985; Kędzior *et al.*, 2025). The stratigraphic architecture of the MS represents an aggrading fluvial system, in which non-incised rivers

deposited fine-grained sediments across extensive alluvial plains. Within this setting, the palaeosols studied occur as thin horizons, developed within a mudstone-dominated succession.

Macroscopic and micromorphological observations indicate that the sections studied represent weakly developed, gleyed Protosols. The soils are generally thin and poorly differentiated, and only in a few cases a well-developed pedogenic structure could be recognized. In many sections, the original sedimentary lamination is still preserved, even at the macroscopic scale, indicating limited pedogenic reworking of the parent material. Root traces confirm *in situ* soil formation, whereas the presence of gley features along with siderites indicate episodes of waterlogging. At the same time, the occurrence of slickensides in some profiles implies that periods of relatively well-drained conditions also occurred. Together, these features indicate fluctuating groundwater levels during soil development.

The limited thickness, weak development of pedogenic features, and preservation of lamination suggest that pedogenesis was repeatedly interrupted by renewed deposition of fine-grained clastic material, thereby resetting the pedogenic processes and preventing the formation of thicker, more mature soil horizons. Such conditions are typical of low-relief floodplain environments, affected by periodic overbank sedimentation (cf., Kraus, 1999). In this setting, the frequency of flooding events and channel avulsions plays a key role in controlling the maturity of palaeosols (e.g., Gibling *et al.*, 2011). The palaeosols are therefore interpreted as alluvial soils, developed on distal floodplain surfaces, relatively distant from the active river channels. Alternatively, some of the parent material may have accumulated in shallow ephemeral ponds that were subsequently colonized by vegetation after the floodwaters retreated.

The frequent occurrence of coal seams directly above the palaeosol horizons indicates intervals of reduced clastic sediment input and increased groundwater levels, which allowed the establishment of mire environments and peat accumulation on the floodplain surface (Cecil *et al.*, 2003). The palaeosol-coal associations therefore record repeated transitions between phases of floodplain stability and phases of peat formation and/or floodplain inundation.

Hydromorphic features vary between profiles. Some palaeosols, contain slickensides, indicating shrink-swell processes. This indicates that these soils initially developed under periodically well-drained conditions, before experiencing a later rise of the local water table that resulted in gleying. In other profiles, gley features are indicated by pedogenic siderite, but no evidence of shrink-swell structures is present. These profiles commonly preserve a thin overlying H horizon (coal layer), suggesting development under more persistently waterlogged conditions. Geochemical redox proxies provide somewhat mixed signals: Mo and V/Cr ratios generally suggest oxic conditions, whereas Th/U ratios indicate some variability in the redox state. These proxies must be interpreted with caution, because they may be influenced by detrital heavy minerals or organic matter. Nevertheless, the presence of pedogenic siderite in sample AP845.5 is consistent with locally reducing conditions, also reflected in a relatively low Th/U ratio (1.15).

The mineralogical maturity of the palaeosols and their geochemical composition indicate that the soil parent material had already undergone significant weathering prior to deposition. Because the soils developed on transported alluvial sediments, the substrate material must have been derived from weathered source areas, located in the upstream part of the palaeocatchment. The examination of trace element ratios would indicate highly weathered material coming from a felsic source. The Sr/Ba ratios varied inversely with base loss, as higher Sr/Ba values occur in more leached horizons (higher leaching – lower base loss; Retallack, 2008; Pereira *et al.*, 2015). The relatively large Rb/Sr ratio (usually >1), along with the relatively small Sr/Ba and Sr/Cu ratios, suggests intense weathering (McLennan *et al.*, 1993; Armstrong-Altrin *et al.*, 2019). Relatively low Sr/Cu ratios, <4 for most of the samples (Fig. 11), also are commonly interpreted as indicators of a warm, humid climate (Jia *et al.*, 2013; Tao *et al.*, 2017). La and Th are immobile chemical elements that concentrate in felsic rocks. Their absolute concentrations and their ratio are very useful indicators of provenance (Cullers *et al.*, 1988; McLennan and Taylor, 1991). Both the absolute contents and the ratio of these elements suggested felsic and intermediate sources (Nath *et al.*, 1997), which is in agreement with the ω - ψ and RW diagrams (Figs 9 and 10). The source area most likely was located southwest of the present position of the USB (Kusiak *et al.*, 2006).

An attempt to constrain the oxygenation state of the soil column can be made on the basis of the Mo content and the V/Cr and Th/U ratios. Mo values <5 ppm would indicate an oxic environment (Crusius *et al.*, 1996), in agreement with the V/Cr ratios below 2 (Jones and Manning, 1994; Nath *et al.*, 1997; Sun *et al.*, 2023). The Th/U ratios suggest variable conditions, as they fluctuate between values that are characteristic for anoxic (<2) and oxic (>2) conditions (Fig. 11; Wignall and Twitchett, 1996; Sun *et al.*, 2023).

All the above-mentioned geochemical proxies should, however, be interpreted cautiously, because they could have been modified by diagenetic processes (cf., Algeo *et al.*, 2025) and/or represent a mixed signal, coming from the depositional environment and detrital input. Furthermore, they are more likely to represent overall catchment-scale weathering processes, rather than *in situ* pedogenesis. In particular, potassium addition, related to the Mesozoic low-temperature hydrothermal event, associated with the rifting of the Tethys and Atlantic oceans, affecting the USB (Środoń *et al.*, 2006), may have shifted the samples toward more felsic fields in these diagrams. Nevertheless, the inferred felsic provenance is consistent with the interpretation of Świerczewska (1995), who suggested that the MS sediments were derived from a recycled orogen, on the basis of sandstone petrography. The most probable source region for both the MS and the overlying Cracow Sandstone Series is therefore the Bohemian Massif (Kusiak *et al.*, 2006).

From a broader perspective, the predominance of weakly developed Protosols within the MS likely reflects relatively frequent flooding and/or channel avulsion during deposition of the MS. Under such conditions, episodes of pedogenesis were frequently interrupted by renewed sedimentation. This contrasts with some other Pennsylvanian basins, such

as the Illinois Basin or the Donets Basin, where thicker and more mature palaeosols have been reported (e.g., Eros *et al.*, 2012; Rosenau *et al.*, 2013). An additional factor contributing to the observed predominance of Protosols in the MS, may be preservation bias: more mature soils may have developed on relatively elevated floodplain surfaces that were subsequently eroded during channel migration.

In a broader stratigraphic context, the recurrent association of palaeosols and coal seams, observed in the MS, reflects a sedimentary motif that is widely documented in Pennsylvanian successions worldwide. Such palaeosol-coal successions are commonly interpreted as records of alternating phases of floodplain stability and mire development, controlled by variations in clastic sediment supply and groundwater level. In many Pennsylvanian basins, these cycles have also been linked to glacio-eustatic sea-level fluctuations, associated with the Late Palaeozoic Ice Age (Heckel, 2008; Eros *et al.*, 2012; Cecil *et al.*, 2014). Although the influence of eustatic forcing may have been reduced in the largely continental USB the studied palaeosols and associated coal seams nevertheless recorded repeated shifts between floodplain pedogenesis and peat-forming wetland environments. A cyclicity connected with the Milanković cycles has been detected in the overlying Cracow Sandstone Series (Laurin *et al.*, 2024) and the older Karvina and Ostrava formations on the Czech side of the basin (Jirásek *et al.*, 2018; Laurin *et al.*, 2024). By interference, a Milanković-type cyclicity can also be expected for the MS. However, the data in the present account are not sufficient to test this hypothesis.

Diagenetic overprint

Due to the known K-metasomatic pulse, geochemical weathering indices involving potassium were generally avoided, as they likely were compromised (cf., Algeo *et al.*, 2025). In the case of RW and ω - ψ metrics that take into account multiple major elements, this effect likely was mitigated. The values of the geochemical indices used in the study (R, CIW, CALMAG, Base loss, ω , and RW) indicate advanced weathering. However, on the basis of palaeosol micromorphology, this weathering must have occurred prior to the deposition of the material. Geochemical proxies, therefore, as well as mineralogy, reflect the overall intensity of weathering during Carboniferous time, not earlier, as is indicated by monazite age spectra (Kusiak *et al.*, 2006), rather than the intensity of *in situ* weathering reactions due to *in situ* pedogenic processes, as discussed above. However, geochemical proxies may have been disrupted by later diagenesis (Algeo *et al.*, 2025). The presence of framboidal pyrite in SEM images confirms at least the intermittent existence of oxygen-deficient conditions. The size of the framboids, close to 10 μm , suggests that the pyrite was formed during early diagenesis in dysoxic conditions (Wilkin *et al.*, 1996). The presence of sulphides and goethite, associated with organic matter, suggest their hydrothermal origin, i.e., these phases likely formed due to interactions with fluids, migrating through the basin in the Triassic (Środoń *et al.*, 2006).

CONCLUSIONS

The Pennsylvanian palaeosols of the Upper Silesian Basin investigated were deposited in valley systems that were frequently flooded. This led to the frequent “rejuvenation” of the palaeosols by the deposition of fresh sediment. Short periods between such events prevented the development of deep, mature, and well-differentiated palaeosols in the Mudstone Series. All palaeosol horizons investigated are relatively immature. However, on the basis of micromorphological features, some present a more advanced stage of pedogenesis than others. Geochemical weathering indices and mineral composition, on the other hand, indicated a high degree of weathering that occurred in the source area of the river sediments, rather than during the pedogenic process. Therefore, mineralogy and geochemical proxies do not reflect the *in situ* weathering in the case of the palaeosols investigated. Caution should be exercised in interpreting geochemical and mineralogical data from palaeosol samples, when no geological or pedological context is available.

Acknowledgements

The work is funded by the National Science Centre, Poland, under the Weave-UNISONO call in the Weave program (project no. 2021/03/Y/ST10/00075) and the Czech National Grant Agency (GAČR) within project 22-11661K. The authors thank Julia McIntosh and an anonymous reviewer, as well as the editors of ASGP, for their comments that significantly improved the manuscript.

Data availability

Supplementary data (XRD patterns), associated with this account, are available at the IGS PAS Data Portal: <https://doi.org/10.60871/INGPAN/8FQUUJ>.

REFERENCES

- Aitchison, J., 1982. The statistical analysis of compositional data. *Journal of the Royal Statistical Society: Series B (Methodological)*, 44: 139–160.
- Algeo, T. J., Hong, H. & Wang, C., 2025. The chemical index of alteration (CIA) and interpretation of ACNK diagrams. *Chemical Geology*, 671: 122474.
- Andrews, E., White, T. & del Papa, C., 2017. Paleosol-based paleoclimate reconstruction of the Paleocene-Eocene Thermal Maximum, northern Argentina. *Palaeogeography, Palaeoclimatology, Palaeoecology*, 471: 181–195.
- Armstrong-Altrin, J. S., Botello, A. V., Villanueva, S. F. & Soto, L. A., 2019. Geochemistry of surface sediments from the northwestern Gulf of Mexico: implications for provenance and heavy metal contamination. *Geological Quarterly*, 63: 522–538.
- Basilici, G., Bo, P. F. D. & de Oliveira, E. F., 2016. Distribution of palaeosols and deposits in the temporal evolution of a semi-arid fluvial distributary system (Bauru Group, Upper Cretaceous, SE Brazil). *Sedimentary Geology*, 341: 245–264.
- Bayon, G., Toucanne, S., Skonieczny, C., André, L., Bermell, S., Cheron, S., Dennielou, B., Etoubleau, J., Freslon, N.,

- Gauchery, T., Germain, Y., Jorry, S. J., Ménot, G., Monin, L., Ponzevera, E., Rouget, M. L., Tachikawa, K. & Barrat, J. A., 2015. Rare earth elements and neodymium isotopes in world river sediments revisited. *Geochimica et Cosmochimica Acta*, 170: 17–38.
- Botor, D., 2020. Burial and thermal history of the Upper Silesian Coal Basin (Poland) constrained by maturity modelling – implications for coalification and natural gas generation. *Annales Societatis Geologorum Poloniae*, 90: 99–123.
- Cecil, B. C., DiMichele, W. A. & Elrick, S. D., 2014. Middle and Late Pennsylvanian cyclothems, American Midcontinent: Ice-age environmental changes and terrestrial biotic dynamics. *Comptes Rendus. Géoscience*, 346: 159–168.
- Cecil, B. C., Dulong, F. T., West, R. R., Stamm, R., Wardlaw, B. & Edgar, N. T., 2003. Climate controls on the stratigraphy of a Middle Pennsylvanian cyclothem in North America. *SEPM Special Publication*, 77: 151–180.
- Cho, T. & Ohta, T., 2022. A robust chemical weathering index for sediments containing authigenic and biogenic materials. *Palaeogeography, Palaeoclimatology, Palaeoecology*, 608: 111288.
- Churchman, G. J. & Lowe, D. J., 2012. Alteration, formation, and occurrence of minerals in soils. In: Huang, P. M., Li, Y. & Sumner, M. E. (eds), *Handbook of Soil Sciences. Vol. 1: Properties and Processes*. CRC Press, Taylor & Francis, Boca Raton, pp. 20.21–20.72.
- Crusius, J., Calvert, S., Pedersen, T. & Sage, D., 1996. Rhenium and molybdenum enrichments in sediments as indicators of oxic, suboxic and sulfidic conditions of deposition. *Earth and Planetary Science Letters*, 145: 65–78.
- Cullers, R. L., Basu, A. & Suttner, L. J., 1988. Geochemical signature of provenance in sand-size material in soils and stream sediments near the Tobacco Root batholith, Montana, USA. *Chemical Geology*, 70: 335–348.
- DiMichele, W. A., Cecil, B. C., Montañez, I. P. & Falcon-Lang, H. J., 2010. Cyclic changes in Pennsylvanian paleoclimate and effects on floristic dynamics in tropical Pangaea. *International Journal of Coal Geology*, 83: 329–344.
- Doebelin, N. & Kleeberg, R., 2015. Profex: a graphical user interface for the Rietveld refinement program BGMN. *Journal of Applied Crystallography*, 48: 1573–1580.
- Doktor, M., 2007. Conditions of accumulation and sedimentary architecture of the upper Westphalian Cracow Sandstone Series (Upper Silesia Coal Basin, Poland). *Annales Societatis Geologorum Poloniae*, 77: 219–268.
- Doktor, M. & Gradziński, R., 1985. Środowisko depozycji aluwialnych utworów węglonośnych serii mułowcowej (górný karbon Zagłębia Górnośląskiego). *Studia Geologia Polonica*, 82: 5–67. [In Polish.]
- Doktor, M. & Gradziński, R., 1999. Środowiska depozycyjne rozpoznane w serii paralicznej Górnośląskiego Zagłębia Węglowego. *Documenta Geonica 1999*. Peres Publishers, Prague, pp. 35–40. [In Polish.]
- Eberl, D. D., 1984. Clay mineral formation and transformation in rocks and soils. *Philosophical Transactions of the Royal Society A – Mathematical Physical and Engineering Sciences*, 311(1517): 241–257.
- Eros, J. M., Montañez, I. P., Osleger, D. A., Davydov, V. I., Nemyrovska, T. I., Poletaev, V. I. & Zhykalyak, M. V., 2012. Sequence stratigraphy and onlap history of the Donets Basin, Ukraine: Insight into Carboniferous icehouse dynamics. *Palaeogeography, Palaeoclimatology, Palaeoecology*, 313–314: 1–25.
- Gibling, M. R., Fielding, C. R. & Sinha, R., 2011. Alluvial valleys and alluvial sequences: Towards a geomorphic assessment. *SEPM Special Publication*, 97: 423–447.
- Gradziński, R., Doktor, M. & Kędzior, A., 2005. Sedimentation of the coal-bearing succession in the Upper Silesia Coal Basin: research trends and the current state of knowledge. *Przegląd Geologiczny*, 53: 734–741. [In Polish, with English summary.]
- Harnois, L., 1988. The CIW index: A new chemical index of weathering. *Sedimentary Geology*, 55: 319–322.
- Heckel, P. H., 2008. Pennsylvanian cyclothems in Midcontinent North America as far-field effects of waxing and waning of Gondwana ice sheets. In: Fielding, C. R., Frank, T. D. & Isbell, J. L. (eds), *Resolving the Late Paleozoic Ice Age in Time and Space. GSA Special Paper*, 441: 275–289.
- Huang, C. M., Retallack, G. J. & Wang, C. S., 2010. Cretaceous calcareous paleosols: pedogenetic characteristics and paleoenvironmental implications. *Acta Pedologica Sinica*, 47: 1029–1038. [In Chinese, with English summary.]
- Jackson, M. L. R., 1969. *Soil Chemical Analysis: Advanced Course*. Published by the author, Madison, Wisconsin, 895 pp.
- Jewuła, K., Kędzior, A., Popa, M. E., Szczerba, M. & Predeanu, G., 2026. Palaeosols, peat, and the shredded climate signal: Time resolution in an Early Jurassic fluvial landscape (Reșița Basin, South Carpathians). *Journal of the Geological Society*, 183: jgs2025–089.
- Jia, J., Liu, Z., Bechtel, A., Strobl, S. A. & Sun, P., 2013. Tectonic and climate control of oil shale deposition in the Upper Cretaceous Qingshankou Formation (Songliao Basin, NE China). *International Journal of Earth Sciences*, 102: 1717–1734.
- Jirásek, J., Opluštil, S., Sivek, M., Schmitz, M. D. & Abels, H. A., 2018. Astronomical forcing of Carboniferous paralic sedimentary cycles in the Upper Silesian Basin, Czech Republic (Serpukhovian, latest Mississippian): New radiometric ages afford an astronomical age model for European biozonations and substages. *Earth-Science Reviews*, 177: 715–741.
- Jirásek, J., Sedláčková, L., Sivek, M., Martinek, K. & Jureczka, J., 2013. Castle Conglomerate Unit of the Upper Silesian Basin (Czech Republic and Poland): A record of the onset of late Mississippian C2 glaciation. *Bulletin of Geosciences*, 88: 893–914.
- Jones, B. & Manning, D. A. C., 1994. Comparison of redox indices used for the interpretation of palaeoredox conditions in ancient mudstones. *Chemical Geology*, 111: 111–129.
- Jureczka, J. & Kotas, A., 1995. Coal deposits. Upper Silesian coal basin. In: Zdanowski, A. & Żakowa, H. (eds), *The Carboniferous system in Poland. Prace Państwowego Instytutu Geologicznego*, 148: 164–173.
- Kahmann, J. A., Seaman, I. J. & Driese, S. G., 2008. Evaluating trace elements as paleoclimate indicators: multivariate statistical analysis of Late Mississippian Pennington Formation paleosols, Kentucky, U.S.A. *The Journal of Geology*, 116: 254–268.
- Kędzior, A., 2016. Reconstruction of an early Pennsylvanian fluvial system based on geometry of sandstone bodies and coal seams: the Zabrze Beds of the Upper Silesia Coal Basin, Poland. *Annales Societatis Geologorum Poloniae*, 86: 437–472.

- Kędzior, A., Gmur, D., Doktor, M. & Opluštíl, S., 2025. Peat formation dynamics in the meandering fluvial system of the Mudstone Series (Middle Pennsylvanian), Upper Silesian Coal Basin, Poland. *Geological Quarterly*, 69: 52.
- Kędzior, A., Gradziński, R., Doktor, M. & Gmur, D., 2007. Sedimentary history of a Mississippian to Pennsylvanian coal-bearing succession: an example from the Upper Silesia Coal Basin, Poland. *Geological Magazine*, 144: 487–496.
- Kotas, A., 1995. Lithostratigraphy and sedimentologic-paleogeographic development, Moravian-Silesian-Cracovian region, Upper Silesian Coal Basin. In: Zdanowski, A. & Żakowa, H. (eds), *The Carboniferous System in Poland. Prace Państwowego Instytutu Geologicznego*, 148: 124–134.
- Kraus, M. J., 1999. Paleosols in clastic sedimentary rocks: their geologic applications. *Earth-Science Reviews*, 47: 41–70.
- Kuligiewicz, A., Środoń, J. & Liivamägi, S., 2021. Oxygen isotopic compositions of end-members in a multicomponent mixture: Ediacaran weathering material from the East European Craton. *Geochimica et Cosmochimica Acta*, 306: 245–262.
- Kusiak, M. A., Kędzior, A., Paszkowski, M., Suzuki, K., González-Álvarez, I., Wajsprych, B. & Doktor, M., 2006. Provenance implications of Th-U-Pb electron microprobe ages from detrital monazite in the Carboniferous Upper Silesia Coal Basin, Poland. *Lithos*, 88: 56–71.
- Laurin, J., Kędzior, A., Naglik, B., Nadłonek, W. & Opluštíl, S., 2024. Eccentricity control on fluvial sedimentation in the tropics during the Middle-Late Pennsylvanian icehouse (~306–314 Ma, Upper Silesian Basin). *Palaeogeography, Palaeoclimatology, Palaeoecology*, 654: 112420.
- Lipp, A. G., Shorttle, O., Syvret, F. & Roberts, G. G., 2020. Major element composition of sediments in terms of weathering and provenance: Implications for crustal recycling. *Geochemistry, Geophysics, Geosystems*, 21: e2019GC008758.
- Mack, G. H., James, W. C. & Monger, H. C., 1993. Classification of paleosols. *GSA Bulletin*, 105: 129–136.
- McIntosh, J. A., Elliott, W. C., Wampler, J. M. & Tabor, N. J., 2023. Identifying detrital and diagenetic minerals in paleosols of the Illinois Basin. *Clays and Clay Minerals*, 71: 722–744.
- McLennan, S., Hemming, S., McDaniel, D. & Hanson, G., 1993. Geochemical approaches to sedimentation, provenance, and tectonics. In: Johnsson, M. L. & Basu, A. (eds), *Processes Controlling the Composition of Clastic Sediments. Geological Society of America, Special Paper*, 284: 21–40.
- McLennan, S. M. & Taylor, S. R., 1991. Sedimentary rocks and crustal evolution: tectonic setting and secular trends. *The Journal of Geology*, 99: 1–21.
- Mehra, O. P. & Jackson, M. L. R., 1960. Iron oxide removal from soils and clays by a dithionite-citrate system buffered with sodium bicarbonate. *Clays and Clay Minerals*, 5: 317–327.
- Nadeau, P. H., 1998. An experimental study of the effects of diagenetic clay minerals on reservoir sands. *Clays and Clay Minerals*, 46: 18–26.
- Nath, B. N., Bau, M., Rao, B. R. & Rao, C. M., 1997. Trace and rare earth elemental variation in Arabian Sea sediments through a transect across the oxygen minimum zone. *Geochimica et Cosmochimica Acta*, 61: 2375–2388.
- Nesbitt, H. W. & Young, G. M., 1982. Early Proterozoic climates and plate motions inferred from major element chemistry of lutites. *Nature*, 299: 715–717.
- Nordt, L. C. & Driese, S. D., 2010. New weathering index improves paleorainfall estimates from Vertisols. *Geology*, 38: 407–410.
- Opluštíl, S. & Cleal, J., 2007. A comparative analysis of some Late Carboniferous basins of Variscan Europe. *Geological Magazine*, 144: 417–448.
- Opluštíl, S., Laurin, J., Hýlová, L., Jirásek, J., Schmitz, M. & Sivek, M., 2022. Coal-bearing fluvial cycles of the late Paleozoic tropics; astronomical control on sediment supply constrained by high-precision radioisotopic ages, Upper Silesian Basin. *Earth-Science Reviews*, 228: 103998.
- Opluštíl, S., Laurin, J., Jureczka, J., Lonek, W. N., Nadłonek, W., Naglik, B., Horák, J., Kędzior, A., Lojka, R., Nádaskay, R. & Sivek, M., 2024. Depositional setting and sequence stratigraphy of Upper Mississippian coal-bearing paralic cyclothems in Upper Silesian foreland. *International Journal of Coal Geology*, 287: 104516.
- Opluštíl, S., Lojka, R., Rosenau, N., Strnad, L. & Kędzior, A., 2019. Climatically-driven cyclicality and peat formation in fluvial setting of the Moscovian–Early Kasimovian Cracow Sandstone Series, Upper Silesia (Poland). *International Journal of Coal Geology*, 212: 103234.
- Ouyang, S., Ashraf, M. A. & Hung, Y.-T., 2019. Application of Rb/Sr ratio in paleo-climate inversion. *Nature Environment and Pollution Technology*, 18: 1713.
- Pereira, C. T., Batezelli, A. & Ladeira, F. S. B., 2015. Paleoprecipitation changes based on paleosols profiles of the Marília Formation (Upper Cretaceous) in the Eastern portion of the Bauru Basin in southeastern Brazil. *Geosciences–Geociências*, 34: 238–257.
- R Core Team, 2024. *R: A Language and Environment for Statistical Computing*. In: R Foundation for Statistical Computing. <https://www.R-project.org/> [31.12.2024].
- Retallack, G. J., 2008. *Soils of the Past: An Introduction to Paleopedology*. John Wiley & Sons, Oxford, 404 pp.
- Rosenau, N. A., Tabor, N. J., Elrick, S. D. & Nelson, W. J., 2013. Polygenetic history of paleosols in Middle-Upper Pennsylvanian cyclothems of the Illinois Basin, U.S.A.: Part I. Characterization of paleosol types and interpretation of pedogenic processes. *Journal of Sedimentary Research*, 83: 606–636.
- Ruxton, B. P., 1968. Measures of the degree of chemical weathering of rocks. *The Journal of Geology*, 76: 518–527.
- Sheldon, N. D. & Tabor, N. J., 2009. Quantitative paleoenvironmental and paleoclimatic reconstruction using paleosols. *Earth-Science Reviews*, 95: 1–52.
- Singer, A., 1980. The paleoclimatic interpretation of clay minerals in soils and weathering profiles. *Earth-Science Reviews*, 15: 303–326.
- Soil Survey Staff, 2022. *Keys to Soil Taxonomy, 13th Edition*. USDA-Natural Resources Conservation Service, 410 pp.
- Środoń, J., 2013. Identification and quantitative analysis of clay minerals. In: Bergaya, F. & Lagaly, G. (eds), *Developments in Clay Science*, 5: 25–49. Elsevier, Amsterdam.
- Środoń, J., Clauer, N., Banaś, M. & Wójtowicz, A., 2006. K-Ar evidence for a Mesozoic thermal event superimposed on burial diagenesis of the Upper Silesia Coal Basin. *Clay Minerals*, 41: 669–690.
- Środoń, J., Paszkowski, M., Drygant, D., Anczkiewicz, A. & Banaś, M., 2013. Thermal history of Lower Paleozoic rocks on the Peri-Tornquist Margin of the East European Craton

- (Podolia, Ukraine) inferred from Combined XRD, K-Ar, and AFT Data. *Clays and Clay Minerals*, 61: 107–132.
- Sun, M., Feng, C. & Li, Y., 2023. Characteristics and paleoenvironment of high-quality shale in the Triassic Yanchang Formation, Southern Margin of the Ordos Basin. *Minerals*, 13: 1075.
- Stoops, G. V., Marcelino, V. & Mees, F. (eds), 2010. *Interpretation of Micromorphological Features of Soils and Regoliths*. Elsevier, Amsterdam, 752 pp.
- Świerczewska, A., 1995. Composition and provenance of Carboniferous sandstones from the Upper Silesia Coal Basin (Poland). *Studia Geologica Polonica*, 108: 27–43.
- Tabor, N. J. & Myers, T. S., 2015. Paleosols as indicators of paleoenvironment and paleoclimate. *Annual Review of Earth and Planetary Sciences*, 43: 333–361.
- Tabor, N. J., Myers, T. S. & Michel, L. A., 2017. Sedimentologist's guide for recognition, description, and classification of paleosols. In: Zeigler, K. & Parker, W. (eds), *Terrestrial Depositional Systems*, Elsevier, pp. 165–208.
- Tao, S., Xu, Y., Tang, D., Xu, H., Li, S., Chen, S., Liu, W., Cui, Y. & Gou, M., 2017. Geochemistry of the Shitoumei oil shale in the Santanghu Basin, Northwest China: Implications for paleoclimate conditions, weathering, provenance and tectonic setting. *International Journal of Coal Geology*, 184: 42–56.
- Trendell, A. M., Nordt, L. C., Atchley, S. C., Leblanc, S. L. & Dworkin, S. I., 2013. Determining floodplain plant distributions and populations using paleopedology and fossil root traces: Upper Triassic Sonsela Member of the Chinle Formation at Petrified Forest National Park, Arizona. *Palaaios*, 28: 471–490.
- Weil, R. R. & Brady, N. C., 2017. *The Nature and Properties of Soils. 15th Edition*. Pearson, New York, 1104 pp.
- Wignall, P. B. & Twitchett, R. J., 1996. Oceanic anoxia and the end Permian mass extinction. *Science*, 272: 1155–1158.
- Wilkin, R. T., Barnes, H. L. & Brantley, S. L., 1996. The size distribution of framboidal pyrite in modern sediments: An indicator of redox conditions. *Geochimica et Cosmochimica Acta*, 60: 3897–3912.
- Zhang, L., Zhang, C. & Dou, L., 2021. Paleoenvironment implication of Red Paleosols in a Late Cretaceous continental succession, Songliao Basin, NE China. *Minerals*, 11: 993.
- Zhang, Z. Y., Huang, L., Liu, F., Wang, M. K., Ndzana, G. M. & Liu, Z. J., 2018. Transformation of clay minerals in nanoparticles of several zonal soils in China. *Journal of Soils and Sediments*, 19: 211–220.